BDNF controls bidirectional endocannabinoid-plasticity at corticostriatal synapses

Giuseppe GANGAROSSA[1 #,*], Sylvie PEREZ[1,#], Yulia DEMBITSKAYA[1], Ilya PROKIN[2,3], Hugues BERRY[2,3] and Laurent VENANCE[1,*]

[1]Dynamics and Pathophysiology of Neuronal Networks Team, Center for Interdisciplinary Research in Biology, College de France, CNRS UMR7241/INSERM U1050, MemoLife Labex Paris, France

[2]INRIA, Villeurbanne, France

[3]University of Lyon, LIRIS UMR5205, Villeurbanne, France

#: co-first authors

[*]Correspondence: giuseppe.gangarossa@univ-paris-diderot.fr and laurent.venance@college-de-france.fr

GG present address: Université Paris Diderot, Sorbonne Paris Cité, Unité de Biologie Fonctionnelle et Adaptative (BFA), CNRS UMR8251, F-75205 Paris, France.

Conflict of interest: the authors have no competing financial interest to declare.

Running title: BDNF controls endocannabinoid-plasticity

ABSTRACT

The dorsal striatum exhibits bidirectional corticostriatal synaptic plasticity, NMDAR- and endocannabinoids-(eCB)-mediated, necessary for the encoding of procedural learning. Therefore, characterizing factors controlling corticostriatal plasticity is of crucial importance. Brain-derived neurotrophic factor (BDNF) and its receptor, the tropomyosine receptor kinase-B (TrkB), shape striatal functions and their dysfunction deeply affect basal ganglia. BDNF/TrkB signaling controls NMDAR-plasticity in various brain structures including striatum. However, despite cross-talks between BDNF and eCBs, the role of BDNF in eCB-plasticity remains unknown. Here, we show that BDNF/TrkB signaling promotes eCB-plasticity (LTD and LTP) induced by rate-based (low-frequency stimulation) or spike-timing-based (spike-timing-dependent plasticity, STDP) paradigm in striatum. We show that TrkB activation is required for the expression and the scaling of both eCB-LTD and eCB-LTP. Using two-photon imaging of the dendritic spines combined with patch-clamp recordings, we show that TrkB activation induces an intracellular calcium boost, thus increasing eCB synthesis and release. We provide a mathematical model for the dynamics of the signaling pathways involved in corticostriatal plasticity. Finally, we show that TrkB activation allows an enlargement of the domain of expression of eCB-STDP. Our results reveal a novel role for BDNF/TrkB signaling in governing eCB-plasticity expression in striatum, and thus the engram of procedural learning.

Key words: striatum, spike-timing dependent plasticity, BDNF, TrkB, endocannabinoids

INTRODUCTION

The striatum, the main input structure of the basal ganglia system, plays a pivotal role in action selection and procedural learning (Yin and Knowlton, 2006; Graybiel and Grafton, 2015). Long-term synaptic plasticity at corticostriatal synapses has been associated with the acquisition of a complex and dynamic behavioral repertoire (Yin et al., 2009; Koralek et al., 2012; Shan et al., 2014; Rothwell et al., 2015; Hawes et al., 2015; Xiong et al., 2015; Ma et al., 2018; Perrin and Venance, 2018). Upon various activity-dependent patterns (rate- or spike-timing-coded), corticostriatal synapses exhibit bidirectional plasticity, LTP and LTD, mediated by NMDA and type-1 cannabinoid receptors (CB1Rs), respectively (Di Filippo et al., 2009; Surmeier et al., 2009; Lovinger, 2010). Thus, identifying factors modulating the expression of activity-dependent plasticity in striatum is of crucial importance.

Emerging evidences suggest that the brain-derived neurotrophic factor (BDNF) and its receptor, the tropomyosine receptor kinase B (TrkB) (Deinhardt and Chao, 2014), are strongly involved in shaping striatal functions (Baydyuk et al., 2011; Besusso et al., 2013; Unterwald et al., 2013; Jing et al., 2017). In addition, alterations of BDNF/TrkB signaling have been observed in several psychiatric and neurodegenerative disorders (Zuccato and Cattaneo, 2009; Autry and Monteggia, 2012). The involvement of BDNF in the expression of (striatal) NMDAR-mediated LTP is now well elucidated (Jia et al., 2010; Park and Poo, 2013; Park et al., 2014). Despite multiple reports revealing functional cross-talks between BDNF and endocannabinoids (eCBs) signaling in the cortex (Huang et al., 2008, Lemtiri-Chlieh and Levine, 2010; Yeh et al., 2017; Maglio et al., 2018), hippocampus (Khaspekov et al., 2004; Roloff et al., 2010), ventral tegmental area (Zhong et al., 2015) and cerebellum (Maison et al., 2009), the role of BDNF in eCB-mediated long-term synaptic plasticity remains largely unknown. Here, we asked whether BDNF/TrkB signaling exerts a control over eCB-plasticity at corticostriatal synapses in the dorsal striatum.

eCBs have emerged as a major signaling system in learning and memory because of their involvement in synaptic plasticity (Castillo et al., 2012; Araque et al., 2017). The eCB system comprises active lipids (mainly 2-arachidonylglycerol, 2-AG, and anandamide) synthesized and released on-demand, which act as retrograde neurotransmitters on presynaptic type-1 cannabinoid receptors (CB1Rs) and postsynaptic transient receptor potential vanilloid-type-1 (TRPV1) (Piomelli, 2003; Piomelli et al., 2007; Di Marzo, 2008; Alger and Kim, 2011). In the dorsal striatum very low levels of BDNF have been reported and the striatal output neurons, the medium-sized spiny neurons (MSNs), do not show detectable level of BDNF mRNA (Altar et al., 1997; Conner et al., 1997). However, MSNs display high levels of TrkB (Baydyuk et al., 2011; Besusso et al., 2013; Unterwald et al., 2013). Striatal BDNF is mainly released from glutamatergic cortical afferents (Altar et al., 1997; Jia et al., 2010). Here, we took advantage of various forms of activity-dependent eCB-plasticity at corticostriatal synapses to investigate the role of BDNF/TrkB signaling in these plasticities. Indeed, in the dorsal striatum, at least three forms of eCB-plasticity have been observed: (*i*) an eCB-LTD induced by a low frequency stimulation (LFS) (Fino et al., 2005; Puente et al., 2011), (*ii*) an eCB spike-timing dependent plasticity (STDP), a spike-timing dependent LTD (t-LTD) induced with 100-150 STDP pairings (Pawlak and Kerr, 2008; Shen et al., 2008; Fino et al., 2010; Paillé et al., 2013), and (*iii*) a eCB-tLTP induced by low numbers of STDP pairings (i.e. 10) (Cui et al., 2015; Cui et al., 2016; Cui et al., 2018; Xu et al., 2018).

Considering the cross-talk between BDNF/TrkB and eCB signaling promoting eCB synthesis (Zhao et al., 2015; Bennett et al., 2017), we questioned the role of TrkB in the expression of eCB-plasticity at corticostriatal synapses. We provide evidence for a novel role of BDNF/TrkB in promoting eCB-mediated synaptic plasticity induced by rate-based or spike-timing-based paradigm. We show that TrkB activation is required for the expression and the scaling of both eCB-LTD and eCB-LTP at the glutamatergic corticostriatal synapse. Using two-photon

imaging at the level of the dendritic elements (spines and shafts) of MSNs combined with patch-clamp recording, our results show that TrkB activation acts as a molecular trigger for boosting intracellular Ca^{2+} transients, thus increasing eCB synthesis and release. We also provide a mathematical model for the dynamics of the signaling pathways involved in striatal plasticity. Combining our experimental results and mathematical modeling, we show that TrkB activation is not only required for eCB-plasticity expression but also for the scaling of the domain of eCB-plasticity expression, in particular in STDP paradigms. Our results reveal a novel role for BDNF/TrkB as a key factor in governing the expression of Hebbian eCB-plasticity in the dorsal striatum.

MATERIALS AND METHODS

Animals

All experiments were performed in accordance with the guidelines of the local animal welfare committee (Center for Interdisciplinary Research in Biology Ethics Committee) and the EU (directive 2010/63/EU). Every precaution was taken to minimize stress and the number of animals used in each series of experiments. OFA rats P_{25-35} (Charles River, L'Arbresle, France) were used for brain slice electrophysiology. Animals were housed in standard 12-hour light/dark cycles and food and water were available *ad libitum*.

Brain slice preparation and patch-clamp recordings

Horizontal brain slices (300-330 µm-thick) containing the somatosensory cortical area and the corresponding corticostriatal projection field (Fino et al., 2005; Cui et al., 2015) were prepared with a vibrating blade microtome (VT1200S, Leica Microsystems, Nussloch, Germany). Corticostriatal connections (between somatosensory cortex layer 5 and the dorso-lateral striatum) are preserved in the horizontal plane. Brains were sliced in a 95% CO2/5% O2-bubbled, ice-cold cutting solution containing (in mM) 125 NaCl, 2.5 KCl, 25 glucose, 25 NaHCO3, 1.25 NaH2PO4, 2 CaCl2, 1 MgCl2, 1 pyruvic acid, and transferred into the same solution at 34°C for one hour and next moved to room temperature. Whole-cell recordings were performed as previously described (Fino et al., 2010; Paillé et al., 2013). For whole-cell recordings, borosilicate glass pipettes of 6-8MΩ resistance were filled with (in mM): 105 K-gluconate, 30 KCl, 10 HEPES, 10 phosphocreatine, 4 Mg-ATP, 0.3 Na-GTP, 0.3 EGTA (adjusted to pH 7.35 with KOH). The composition of the extracellular solution was (mM): 125 NaCl, 2.5 KCl, 25 glucose, 25 $NaHCO_3$, 1.25 NaH_2PO_4, 2 $CaCl_2$, 1 $MgCl_2$, 10 µM pyruvic acid bubbled with 95% O_2 and 5% CO_2. Signals were amplified using EPC10-2 amplifiers (HEKA Elektronik, Lambrecht, Germany). All recordings were performed at 34°C, using a temperature

control system (Bath-controller V, Luigs & Neumann, Ratingen, Germany) and slices were continuously superfused with extracellular solution, at a rate of 2 ml/min. Slices were visualized under an Olympus BX51WI microscope (Olympus, Rungis, France), with a 4x/0.13 objective for the placement of the stimulating electrode and a 40x/0.80 water-immersion objective for the localization of cells for whole-cell recordings. Current- and voltage-clamp recordings were sampled at 10 kHz, with the Patchmaster v2x32 program (HEKA Elektronik).

Synaptic plasticity induction protocols

Electrical stimulations were performed with a concentric bipolar electrode (Phymep, Paris, France) placed in layer 5 of the somatosensory cortex. Electrical stimulations were monophasic, at constant current (ISO-Flex stimulator, AMPI, Jerusalem, Israel). Currents were adjusted to evoke 100-300 pA EPSCs. Repetitive control stimuli were applied at 0.1 Hz.

Low frequency stimulation protocols

Low-frequency stimulation (LFS) consisted in 600 cortical stimuli at 1 Hz and was performed in a Hebbian mode; Indeed, the depolarization of the postsynaptic element from its resting membrane potential (RMP) to 0 mV was coincident with the presynaptic stimulation.

Spike-timing-dependent plasticity protocols

STDP protocols consisted of pairings of pre- and postsynaptic stimulations (at 1 Hz) separated by a specific time interval (Δt_{STDP}). Presynaptic stimulations corresponded to cortical stimulations and the postsynaptic stimulation of an action potential evoked by a depolarizing current step (30 ms duration) in MSNs. The STDP protocol involved pairing pre- and postsynaptic stimulation with a certain fixed timing interval, Δt_{STDP} ($\Delta t_{STDP}<0$ indicating that postsynaptic stimulation preceded presynaptic stimulation, i.e. post-pre pairings, and $\Delta t_{STDP}>0$ indicating that presynaptic stimulation preceded postsynaptic stimulation, i.e. pre-post pairings), repeated n times at 1 Hz. eCB-tLTD was induced with 100 pre-post pairings with

$10<\Delta t_{STDP}<20$ ms and eCB-tLTP was induced with 10 post-pre pairings with $-20<\Delta t_{STDP}<-10$ ms as previously described (Cui et al., 2015; Cui et al., 2016; Xu et al., 2018). Recordings were made over a period of 10 minutes at baseline, and for at least 40 minutes after the STDP induction protocols; long-term changes in synaptic efficacy were measured for the last 10 minutes. We individually measured and averaged 60 successive EPSCs, comparing the last 10 minutes of the recording with the 10-minute baseline recording. Neuron recordings were made in in voltage-clamp mode during baseline and for the 50-60 minutes of recording after the STDP protocol. Variation of input and access resistances, measured every 10 sec all along the experiment, beyond 20% led to the rejection of the experiment.

Electrophysiological data analysis

Off-line analysis was performed with Fitmaster (Heka Elektronik), Igor-Pro 6.0.3 (Wavemetrics, Lake Oswego, OR, USA) and custom-made software in Python 3.0. Statistical analysis was performed with Prism 5.02 software (San Diego, CA, USA). In all cases "n" refers to an experiment on a single cell from a single slice. All results are expressed as mean ± SEM. Statistical significance was assessed by two-tailed student *t*-tests (unpaired or paired *t*-tests) or one-way ANOVA (with Newman-Keuls post hoc test) when appropriate, using the indicated significance threshold (*p*).

Two-photon imaging combined with whole-cell recordings

Whole-cell patch-clamp pipettes (6-8 MΩ) were filled with the solution (in mM): 122 K-gluconate, 13 KCl, 10 HEPES, 10 phosphocreatine, 4 Mg-ATP, 0.3 Na-GTP, 0.3 EGTA (adjusted to pH 7.35 with KOH). Morphological tracer Alexa Fluor 594 (50 μM) and Ca^{2+}-sensitive dye Fluo-4F (250 μM) were added to the intracellular solution to monitor Ca^{2+} transients. Cells were filled with the dyes for at least 15 min to ensure dye equally distributed

and visually identified under Scientifica TriM Scope II system (LaVision, Germany), with a 60x/1.00 water-immersion objective. Alexa Fluor 594 and Fluo-4F were excited at 830 nm wavelength (femtoseconds IR laser Chameleon MRU-X1, Coherent, UK), and their fluorescence were detected with photomultipliers within 525/50 and 620/60 nm ranges, respectively. Line-scan imaging at 200 Hz was performed to obtain Ca^{2+} signals in the dendritic shaft and spines and was synchronized with patch-clamp recordings. In each recording we injected a prolonged somatic depolarization and monitored maximal Ca^{2+} elevations to verify linear dependence of Fluo-4F Ca^{2+} signals (nonlinearity was below 20%) and that Ca^{2+} transients were below saturation level. The changes in baseline Ca^{2+} level were monitored as the ratio between the baseline Fluo-4F and Alexa Fluor 594 fluorescence. If this ratio increased during the experiment for more than 20%, the cell was discarded. The dark noise of the photomultipliers was collected when the laser shutter was closed in every recording. We chose to examine the τ decay constant of Ca^{2+} response (τCa^{2+}) and not the calcium amplitude because of run-down phenomenon.

Two back-propagating action potentials (bAPs) evoked by a depolarizing current step (30 ms duration) have been used to monitor Ca^{2+} transients either in an unpaired manner (i.e. bAPs only) or paired with cortical stimulation (post-pre or pre-post paired stimulations). The excitability was measured in current-clamp mode by 500 ms steps of current injections from -300 to +500 pA with step of 20 pA to verify the identity of the cell and measure input resistance. Input and series resistances were routinely measured in voltage-clamp mode and data were discarded if resistances changed by more than 20% during the recording. Signals were amplified using with EPC10-2 amplifiers (HEKA Elektronik, Lambrecht, Germany). All recordings were performed at 34°C (Bath-controller-V, Luigs & Neumann, Ratingen, Germany) and slices were continuously superfused with extracellular solution, at a rate of 2

ml/min. Recordings were sampled at 10 kHz with the Patchmaster v2x32 program (HEKA Elektronik).

Electrophysiological data were analyzed with Fitmaster (Heka Elektronik) and custom-made software in Python 3.0. Ca^{2+} transients were analyzed with custom made software in Python 3.0 and averaged in MS Excel (Microsoft, USA). The measurements of Ca^{2+} transient were represented as ΔG/R: $(G_{peak}-G_{baseline})/(R_{baseline}-R_{dark\ noise})$. Baseline Ca^{2+} signals were represented by baseline G/R, $(G_{baseline}-G_{dark\ noise})/(R_{baselin-Rdark\ noise})$, where G is the Fluo-4F fluorescence, and R is Alexa Fluor 594 fluorescence. $G_{baseline}$, $R_{baseline}$ and G_{peak} were obtained from the parameters of the bi-exponential fitting model in each trial and then averaged between 5-6 repetitions for each condition. $G_{dark\ noise}$ and $R_{dark\ noise}$ are the dark currents of the corresponding photomultipliers. For illustration purposes, traces result from the average of five sequential traces. The statistical significance was tested using a paired or unpaired Student's t-test in Prism 5.02 software (San Diego, CA, USA). The data are given in mean ± SEM where ''n'' designates the number of recordings.

Chemicals

N-(piperidin-1-yl)-5-(4-iodophenyl)-1-(2,4-dichlorophenyl)-4-methyl-1H-pyrazole-3-carboxamide (AM251, 3μM) (Tocris) was dissolved in ethanol and then added in the external solution at a final concentration of ethanol of 0.015%. N-[2-[[(Hexahydro-2-oxo-1H-azepin-3-yl)amino]carbonyl]phenyl]benzo[b]thiophene-2-carboxamide (ANA12, 10 μM) (Tocris), (9S,10R,12R)-2,3,9,10,11,12-Hexahydro-10-hydroxy-9-methyl-1-oxo-9,12-epoxy-1H-diindolo[1,2,3-fg:3',2',1'-kl]pyrrolo[3,4-i][1,6]benzodiazocine-10-carboxylic acid methyl ester (K252a, 200 nM) (Tocris), 7,8-Dihydroxy-2-phenyl-4H-1-benzopyran-4-one (DHF, 10 μM) (Tocris), 1,4-Diamino-2,3-dicyano-1,4-bis(2-aminophenylthio)-butadiene (U0126, 10μM) (Tocris) and 2-(4-morpholino)-8-phenyl-4H-1-benzopyran-4-one (LY294002, 10μM) (Tocris)

were dissolved in DMSO and then added in the external solution at a final concentration of DMSO of 0.001-0.04%. DMSO (0.001-0.04% final concentration) was used as control for all the experiments. None of the bath-applied drugs had a significant effect on basal synaptic transmission. The normalized $EPSC_{(baseline\text{-}drugs/baseline\text{-}control)}$ amplitude were (in %): 97±4 for K252a (200 nM) (n=14, p=0.6790), 101±5 for ANA12 (10 μM) (n=12, p=0.8001), 97±2 for DHF (10 μM) (n=11, p=0.4937) and 100±1 for U0126 (10 μM) co-applied with LY294002 (10 μM) (n=5, p=0.2588).

Mathematical modeling

To account for TrkB signaling in the postsynaptic neuron, the mathematical model of STDP at corticostriatal synapses previously described (Cui et al, 2016) was extended. We refer to Cui et al. (2016) for a complete description of the model and its parameters, and here we give a broad outline of the model, together with a detailed description of the modifications we implemented in the present study. Cui et al. (2016) considers an isopotential electrical model of the postsynaptic membrane potential coupled to a detailed description of postsynaptic signaling pathways, including calcium currents, the activation of CaMKIIα and the production of endocannabinoids (Fig. 5A). Each presynaptic stimulus *i* of the STDP protocol triggers a surge of glutamate concentration in the synaptic cleft, $G(t)$, modeled as an immediate increase followed by exponential decay:

$$G(t) = G_{\max} \sum_i \exp\left(-\frac{t-t_{pre_i}}{\tau_G}\right) \Theta\left(t - t_{\mathrm{pre}_i}\right) \quad (1)$$

where t_{pre_i} is the time of the presynaptic stimulus and the Heaviside function $\Theta(x) = 1$ if $x \geq 0$, 0 otherwise. Postsynaptic stimulations of the STDP induction protocol give rise to action currents that combine the step-current injected in the postsynaptic soma at time t_{post_i} and the resulting action potential:

$$I_{\text{action}}(t) = -\text{DC}_{\text{max}} \sum_{\text{i}} R\left(t, t_{\text{post}_i}, \text{DC}_{\text{dur}}\right) - \text{AP}_{\text{max}} \sum_{\text{i}} \Theta\left(t - \delta - t_{\text{post}_i}\right) \exp\left(\frac{-t+\delta+t_{\text{post}_i}}{\tau_{\text{bAP}}}\right) \quad (2)$$

where $R(t, a, l) = \Theta(t - a) - \Theta(t - a - l)$ and δ accounts for the time elapsed between the onset of the postsynaptic step current and the action potential (~3ms in MSNs). The model describes the resulting electrical response of an isopotential postsynaptic element endowed with AMPAR, NMDAR, VSCC and TRPV1 conductances:

$$\begin{aligned} C_{\text{m}} \frac{\text{d}V}{\text{d}t} &= -g_L(V - V_{\text{L}}) - I_{\text{AMPAR}}(V, G(t)) - I_{\text{NMDAR}}(V, G(t)) \\ &\quad - I_{\text{VSCC}}(V) - I_{\text{TRPV1}}(V, AEA) - I_{\text{action}}(t) \end{aligned} \quad (3)$$

where V is the postsynaptic membrane potential and AEA stands for anandamide concentration. The mathematical expressions used for the currents of eq. (3) are given in Cui et al. (2016).

The dynamics of free cytosolic calcium C was computed according to:

$$T_{\text{C}}(C) \frac{dC}{dt} = J_{IP_3R} - J_{\text{SERCA}} + J_{\text{leak}} + J_{\text{NMDAR}} + J_{\text{VSCC}} + J_{\text{TRPV1}} - \frac{C - C_{\text{b}}}{\tau_{C_{\text{b}}}} \quad (4)$$

where J_{NMDAR}, J_{VSCC} and J_{TRPV1} are the calcium fluxes from the respective plasma membrane channels (eq. 3). $T_{\text{C}}(C)$ is a time scaling factor accounting for the presence of endogenous calcium buffers. The terms J_{IP_3R}, J_{leak} and J_{SERCA} describe calcium exchange flows between the cytosol and the endoplasmic reticulum (ER) via IP3-Receptor channels (IP3R), passive ER-to-cytosol leak and Sarcoplasmic/Endoplasmic Reticulum $Ca2^{+}$-ATPases (SERCA).

Inositol 1,4,5-trisphosphate (IP3) and diacylglycerol (DAG) are central signaling molecules in the model because they activate IP3R, thus increasing cytosolic Ca and allow the formation of 2-arachidonoylglycerol (2-AG) by calcium-activated DAG Lipase-α. Their dynamics is modeled as:

$$\frac{\text{d}IP_3}{\text{d}t} = \frac{v_\beta G}{G + K_R + \frac{K_P C}{(K_\pi + C)}} + \frac{v_\delta}{1 + \frac{IP_3}{\kappa_d}} \frac{C^2}{K_\delta^2 + C^2} - v_{3\text{K}} CaMKII_{\text{act}} \frac{IP_3}{K_3 + IP_3} - r_{5\text{P}} IP_3 + v_{\text{TrkB}} \quad (5)$$

and

$$\frac{\mathrm{d}DAG}{\mathrm{d}t} = \frac{v_\beta G}{G+K_R+\frac{K_P C}{(K_\pi+C)}} + \frac{v_\delta}{1+\frac{IP_3}{\kappa_d}} \frac{C^2}{K_\delta^2+C^2} - \frac{r_{DGL} DAGL \cdot \varphi_{DAGL} \cdot DAG}{K_{DAGL}+DAG} - r_{\mathrm{DAGK}} DAG + v_{\mathrm{TrkB}} \quad (6)$$

In both eq. (5) and (6), the first two terms of the right-hand size member correspond to IP_3 and DAG synthesis via mGluR-activated PLCβ and Ca-activated (agonist independent) PLCδ. The third and fourth terms of the right-hand size member account for IP_3 consumption by active CaMKII ($CaMKII_{\mathrm{act}}$) and Inositol 5-Phosphatase (eq. 5) or DAG consumption by DAG Lipase and DAG kinase (eq. 6).

The last term of eq. (5) and (6), i.e. v_{TrkB} constitutes the main modification of the model implemented in the present study (i.e. v_{TrkB}=0 in Cui et al. 2016). This term represents a constant production of IP_3 and DAG by TrkB and accounts, using the simplest formulation, for TrkB-triggered activation of PLCγ. Therefore, our model includes the effect of BDNF and TrkB on IP_3 and DAG production by PLCγ, thus disregarding any other potential effects on corticostriatal plasticity (mitogen-activated protein kinase, MAPK, or phosphatidylinositol 3-kinase, PI3K, pathways).

Our model also accounts for the biochemical pathways leading to the production of the endocannabinoids 2-AG and AEA, and their subsequent activation of cannabinoid receptors type-1, CB_1R (see Fig. 5A). In agreement with experimental observation (Cui et al, 2015), CB_1R activation in the model sets the synaptic weight W in a biphasic way: moderate amount CB_1R activation decrease W while large amounts of CB_1R activation increase it. This principle was modeled using a phenomenological expression:

$$\Omega(y_{\mathrm{CB1R}}) = \begin{cases} 1 + A_{LTP}, & \text{if } \theta_{\mathrm{LTD}}^{\mathrm{start}} < y_{\mathrm{CB1R}} < \theta_{\mathrm{LTD}}^{\mathrm{stop}}, \\ 1 - A_{LTD}, & \text{if } y_{\mathrm{CB1R}} > \theta_{\mathrm{LTP}}^{\mathrm{start}}, \\ 1, & \text{otherwise.} \end{cases} \quad (7)$$

where $\theta_{\mathrm{LTD}}^{\mathrm{start}}$, $\theta_{\mathrm{LTD}}^{\mathrm{stop}}$ and $\theta_{\mathrm{LTP}}^{\mathrm{start}}$ are plasticity thresholds and y_{CB1R} is proportional to the fraction of activated CB1R. Finally, the function $\Omega(y_{\mathrm{CB1R}})$ sets the synaptic weight W according to:

$$\frac{d\mathrm{W}}{dt} = \frac{\Omega(y_{\mathrm{CB1R}}) - \mathrm{W}}{\frac{P_1}{P_2^{P_3} + (y_{\mathrm{CB1R}} + P_5)^{P_3}} + P_4}, \tag{8}$$

Parameters and numerics

We set the values of almost all the model parameters to their values in Cui et al (2016), except for 6 parameters related to IP_3 and DAG dynamics, that we altered to account for the addition of v_{TrkB} in eq. (5) and (6) above: ($v_{\mathrm{TrkB}}, \kappa_d, K_\delta, K_R, v_\delta, CaM_{\mathrm{tot}}$), representing respectively the rate of production of IP_3 by TrkB, PLCδ product inhibition, PLCδ Ca-activation, glutamate affinity to mGluR, PLCδ maximal rate and the total concentration of calmodulin. Estimation of those 6 parameters was achieved using Differential Evolution (pagmo2 python library) to minimize the least-square distance between model outputs and experimental measurements of W_{total} obtained with various values of the STDP protocol parameters (N_{pairings}, Δt_{STDP}, S_{TrkB}). Here S_{TrkB}={DHF, ANA12, Ctrl} specifies the pharmacology used against TrkB, i.e. addition of DHF/TrkB agonist, addition of ANA12/TrkB antagonist or no addition. To reflect the importance of eCB-tLTP in our study, the weights of the corresponding data points (i.e. N_{pairings}=25, Δt_{STDP}=-15 ms) were fivefold that of the other data points. The estimated parameter values were κ_d=0.0623 μM, K_γ=0.3514 μM, K_R=4.9999 μM, v_δ=0.0209 μM/s, CaM_{tot}=0.0714 μM and v_{TrkB} =0.010 μM/s (S_{TrkB}=Ctrl), 0.000 μM/s (S_{TrkB}=ANA12) or 0.015 μM/s (S_{TrkB}=DHF).

Numerical integration was performed as detailed in Cui et al (2016), i.e. using the ODEPACK LSODA solver compiled from fortran77 for python with f2py. Initial conditions were set to the steady-state of each variable in the absence of stimulation.

RESULTS

To examine the effect of BDNF onto eCB-mediated corticostriatal plasticity, we performed whole-cell recordings from MSNs of the dorsolateral striatum in horizontal brain slices at postnatal days P_{25-35} (Fig. 1A, 1B). We investigated the involvement of TrkB activation in bidirectional eCB-plasticity induced by three distinct Hebbian activity patterns: (*i*) the eCB-LTD induced by a low frequency stimulation (LFS) protocol (600 cortical stimulations at 1 Hz) (Fino et al., 2005; Puente et al., 2011), (*ii*) the eCB-tLTD induced with 100 STDP pairings (Shen et al., 2008; Fino et al., 2010; Paillé et al., 2013; Cui et al., 2015) and (*iii*) the eCB-tLTP induced by low numbers of STDP pairings (*i.e.* ~10) (Cui et al., 2015; Cui et al., 2016; Cui et al., 2018; Xu et al., 2018).

TrkB activation is necessary for eCB-LTD induced by low frequency stimulation (LFS)

The LFS protocol consisted in 600 cortical stimuli at 1 Hz with concomitant depolarization (50 ms) of the recorded MSNs (Fig. 1B) and induced reliable LTD (LFS-LTD), in line with previous studies (Fino et al., 2005; Puente et al., 2013). An example of LFS-LTD recorded during one hour after LFS is shown in Figure 1C; Input resistance (Ri) remained stable over this period. Overall, LFS induced LTD (mean value of EPSC amplitude recorded 50 min after LFS protocol induction: 47±8%, n=7, p=0.0005). This striatal LFS-LTD was CB_1R-mediated since prevented by AM251 (3μM), a specific CB_1R inhibitor (97±9%, n=6, p=0.7729) (Fig. 1D).

We then investigated whether TrkB activation was required for the induction of the LFS-LTD. Bath-applied K252a (200 nM), a selective inhibitor of the tyrosine kinase activity of the Trk family, prevented LFS-LTD. Figure 1E shows an example of the absence of synaptic plasticity with K252a. In summary, K252a prevented the induction of LFS-LTD (91±7%, p=0.2101, n=8) (Fig. 1F and 1H). To confirm this finding, we then used ANA12 (10 μM), a specific TrkB

inhibitor, structurally distinct from K252a. In the example shown in the Figure 1G, LFS with bath-applied ANA12 failed to induce LTD. In summary, we observed that ANA12 prevented the induction of LFS-LTD (100±10%, p=0.9725, n=9) (Fig. 1F and 1H).

Altogether our results demonstrate that TrkB activation is necessary for LFS-eCB-LTD expression (Fig. 1H). (Fig. 1H; One-way ANOVA p=0.0007).

STDP-induced eCB-tLTD requires TrkB activation

We next tested whether TrkB activation was necessary for another form of eCB-LTD, a spike-timing-dependent LTD (tLTD). This plasticity is induced with a STDP protocol consisting in pairing the pre- and postsynaptic stimulations separated by a fixed temporal interval, Δt_{STDP}, repeated here 100 times at 1 Hz (with Δt_{STDP}~15ms) (Fig. 2A). We have previously shown that GABA operates as a Hebbian/anti-Hebbian switch at corticostriatal synapses (Paillé et al., 2013; Valtcheva et al., 2017) and corticostriatal STDP polarity depends on the presence (*in vitro* Hebbian STDP; Pawlak and Kerr, 2008; Shen et al., 2008) or absence (*in vitro* anti-Hebbian STDP; Fino et al., 2005; Fino et al., 2010; Cui et al., 2015; *in vivo* anti-Hebbian STDP; Schulz et al., 2010) of $GABA_A$ receptor antagonists. As exemplified in Supplementary Figure 1A, we observed that 100 pre-post pairings triggered corticostriatal tLTD. Overall, 100 pre-post pairings induced tLTD (68±7%, p=0.0010, n=10), which was CB_1R-mediated since AM251 (3μM) fully prevented tLTD expression (103±7%, p=0.5917, n=5) (Fig. 2B), in agreement with previous results (Pawlak and Kerr, 2008; Shen et al., 2008; Fino et al., 2010; Cui et al., 2015).

We next investigated whether the activation of TrkB was required for the induction of the eCB-tLTD. K252a (200 nM) application prevented eCB-tLTD expression, as exemplified in the Supplementary Figure 1B. Overall, K252a prevented eCB-tLTD (105±8%, p=0.5847, n=9) (Fig. 2C and 2D). Similarly, ANA12 (10 uM) prevented eCB-tLTD, as exemplified in the

Supplementary Figure 1C. In summary, ANA12 abolished eCB-tLTD expression (101± 9%, *p*=0.9699, n=10) (Fig. 2C and 2D). Altogether this set of results reveals that eCB-tLTD is dependent on the activation of TrkB (Fig. 2D; One-way ANOVA *p*=0.0073).

STDP-induced eCB-tLTP requires TrkB activation

We have previously reported that low numbers of STDP pairings (~10) induce an eCB-tLTP, a form of plasticity dependent on the activation of CB_1R at corticostriatal synapses in the dorsolateral striatum (Cui et al., 2015; Cui et al., 2016; Cui et al., 2018; Xu et al., 2018). We thus tested whether the involvement of TrkB was crucial not only in eCB-mediated depression (LFS-eCB-LTD and eCB-tLTD) but also in eCB-tLTP. 10 post-pre pairings at 1 Hz (Fig. 3A) induced tLTP as exemplified in Supplementary Figure 1D. Overall, 10 post-pre STDP pairings induced tLTP (153±21%, *p*=0.0021, n=9), which was prevented by AM251 (3μM) (77±9%, p=0.0508, n=6) (Fig. 3B).

Blockade of TrkB by K252a (200 nM) prevented eCB-tLTP induction, as exemplified in Supplementary Figure 1E. Overall, K252 prevented the induction of eCB-tLTP and even induced tLTD (74±5%, *p*=0.0006, n=10) (Fig. 3F). Using ANA12, we also observed that 10 post-pre pairings did not induce tLTP, as exemplified in the Supplementary Figure 1F. In summary, ANA12 prevented eCB-tLTP (97±4%, *p*=0.4827, n=7) (Fig. 3C and 3D). Altogether these results show that BDNF/TrkB signaling is necessary for corticostriatal eCB-tLTP (Fig. 3D; One-way ANOVA p=0.0003).

In conclusion, bidirectional eCB-mediated plasticity, i.e. eCB-LTD (induced by LFS or STDP induction protocol) as well as eCB-tLTP (induced with low numbers of STDP pairings), is dependent on TrkB activation.

Activation of TrkB boosts calcium transients

eCBs (2-AG and AEA) are synthesized and released on-demand (Alger and Kim, 2011). Enzymes involved in eCB biosynthesis exhibit a tight dependence on cytosolic calcium and consequently eCB-mediated plasticity strongly relies on calcium dynamics (Piomelli, 2003; Chevaleyre et al., 2006, Heifets and Castillo, 2015). It exists a link between TrkB intracellular signaling pathways and calcium dynamics via the activation of the PLC signaling pathway, and more precisely PLCγ (Hashimotodani et al., 2005).

Here, we examined whether TrkB activation induced a change in cytosolic calcium transients, which could account for its involvement in eCB-mediated plasticity. We monitored Ca^{2+} transients in dendritic spines and adjacent shafts using two-photon microscopy in line-scan mode (Fig. 4A1 and A2) using ratiometric indicators Fluo-4F (250μM) and Alexa Fluor 594 (50μM) (Fig. A3). We examined calcium transients under TrkB activation (using the specific TrkB agonist DHF, 10μM) while eliciting either two back-propagating action potentials (bAPs) without presynaptic paired stimulation (Fig. 4B), or pairing one corticostriatal EPSP with two bAPs for Δt~+15ms (Fig. 4C) or for Δt~-15ms (Fig. 4D).

First, during unpaired postsynaptic stimulation (bAPs only) we found that application of DHF increased the decay τ constant of Ca^{2+} response (τCa^{2+}) to 124±5% of control (n=7, p=0.0060) in spines whereas no changes of τCa^{2+} was observed in adjacent dendritic shafts (112±6% of control, n=7, p=0.0943) (Fig.4B). We next pre-treated with ANA12 (10 μM) and then applied DHF to ensure that DHF-induced effects on τCa^{2+} were TrkB-mediated (Supplementary Fig. 2A). In both spines and shafts, we observed that τCa^{2+} remained unaffected after ANA12 application (spines: 103±3%, n=8, p=0.3099; shafts: 103±1%, p=0.0516) or after ANA12+DHF co-application (spines: 102±4% of control, p=0.8776; shafts: 108±2%, p=0.0704). Since DHF and ANA12 were dissolved in DMSO (0.02-0.04% final concentration), we tested the effects of DMSO alone to ensure the specificity of the DHF and ANA12 effects (Supplementary Fig. 2B). In spines and shafts we found no significant difference in τCa^{2+} between control and

DMSO (spines: 100±3% n=7, p=0.9882; shafts: 103±4%, p=0.4444) (ANOVA test: control and DMSO).

Second, we applied paired stimulations consisted of cortical stimulation followed by postsynaptic bAPs (Δt~+15ms), i.e. a pre-post pairings as used for eCB-tLTD induction (Fig. 4C). Under DHF application, pre-post pairings induced an increase in τCa^{2+} in dendritic spines to 111±3% when compared to control (n=8, p=0.0085) (Fig. 4C). In dendritic shafts, we did not observe significant changes in τCa^{2+} (106±3%, n=8, p=0.0847) (Fig. 4C). In both dendritic spines and shafts, we found that τCa^{2+} were not modified by ANA12 treatment (spines: 104±3%, n=6, p=0.1975; shafts: 98±2%, p=0.4030) or when ANA12 and DHF were co-applied (spines: 105±7%, p=0.8731; shafts: 99±6%, p=0.7712) (Supplementary Fig. 4C).

Third, we tested whether post-pre pairings yielded similar results than with bAPs only or with pre-post STDP pairings (Fig. 4D). To do so, we applied pairings consisting of postsynaptic bAPs followed by cortical stimulation (Δt~-15ms). Under DHF application, post-pre pairings induced an increase in τCa^{2+} in dendritic spines to 112±5% compared to control (n=7, p=0.0391) (Fig. 4D). In dendritic shafts, we did not observe significant changes in τCa^{2+} (109±5%, n=7, p=0.0941) (Fig. 4D).

Altogether these results indicate that TrkB activation modifies the dynamics of the Ca^{2+} transients (triggered by bAPs only, pre-post or post-pre STDP pairings), and promotes longer Ca^{2+} events with higher quantity of intracellular calcium. This increased calcium signaling upon TrkB activation can be viewed as a necessary boost to favor the synthesis and release of eCBs.

Predicting the effect of TrkB activation on eCB-STDP with a mathematical model

We questioned how TrkB activation could participate to eCB-tLTD and eCB-tLTP, depending on the activity pattern of either side of the synapse. To address this question, we built a

mathematical model of the molecular mechanisms of corticostriatal synaptic plasticity (Fig. 5A). Our model is based on the NMDAR- and CB_1R- signaling pathways involved in corticostriatal STDP (Pawlak and Kerr, 2008; Shen et al., 2008; Fino et al., 2010; Paillé et al., 2013; Cui et al., 2015) and actually extends to TrkB signaling the mathematical model we validated in previous studies (Cui et al., 2016; Cui et al., 2018; Xu et al., 2018). It expresses the kinetics of the enzymes and binding reactions implicated, including the effects of AMPAR, NMDAR, VSCC and TRPV1, on cytosolic Ca^{2+}, IP_3-controled Ca^{2+}-induced Ca^{2+} release from the endoplasmic reticulum, the synthesis of endocannabinoids (2-AG and AEA) via diacylglycerol (DAG) lipase α and FAAH pathways, respectively, and the retrograde activation of presynaptic CB_1R (Fig. 5A). In agreement with experimental evidence (Cui et al., 2015; Cui et al., 2016; Cui et al., 2018; Xu et al., 2018), CB_1R activation sets the value of the synaptic weight W in the model according to a biphasic mechanism: moderate amounts of CB_1R activation yield LTD whereas high level of CB_1R activation yields LTP. Note that such a concentration-dependent biphasic control of the signaling pathway downstream of CB_1R has consistently been evidenced *in vitro* (Glass et al., 1997, Jarrahian et al., 2004, Kearn et al., 2005, Eldeeb et al., 2016).

Our model contains three isoforms of phospholipase-C (PLCβ, δ and γ) in the postsynaptic neuron: PLCβ is activated by binding of presynaptically-released glutamate to mGluR, a $G_{q/11}$-coupled GPCR; PLCδ is agonist-independent but tightly controlled by cytosolic Ca^{2+}; and PLCγ is activated by TrkB (Fig. 5A). In spite of those distinct properties, the three PLC catalyze the same reaction: the synthesis of inositol triphosphate (IP_3) and DAG from phosphatidylinositol biphosphate (PIP2). In turn, IP_3 activates IP3-receptor channels at the membrane of the endoplasmic reticulum, which boost the calcium influx in the cytosol. Model predictions show that the transient Ca^{2+}response to glutamate release upon presynaptic stimulation is wider (and slightly larger) when TrkB is activated when compared to control conditions (Fig. 5B), whereas

it remains unchanged upon TrkB inhibition (Fig. 5B). This behavior matches the calcium two-photon imaging experiments reported in the Figure 4 with the use of TrkB agonist and antagonist, DHF and ANA12, respectively.

In control conditions (Fig. 5C1), the model reproduces the characteristics of eCB-STDP expression: eCB-tLTD starts to be expressed when at least 25 pre-post stimulations are applied (with $\Delta t \sim +20$ms) and progressively reinforces when $N_{pairings}$ increases. eCB-tLTP is observed for low numbers of post-pre pairings ($N_{pairings} \in [2,20]$, $\Delta t \sim -15$ms) and disappears after 20 pairings.

In the model, the activation of TrkB (Fig. 5C2) has two main effects following STDP induction protocols: (*i*) the eCB-tLTP region (red region in Fig. 5C2) expands considerably in terms of Δt and $N_{pairings}$ and (*ii*) eCB-tLTD is more pronounced (i.e. the blue regions of tLTD in Fig. 5C2 are darker than those in Fig. 5C1). On the opposite, the inhibition of TrkB precludes the induction of eCB-tLTP (note the lack of red region in Fig. 5C3) and considerably weakens eCB-tLTD (Fig. 5C3). Comparison of model outputs with experimental data can be carried out for the ($N_{pairings}$, Δt) values that were tested experimentally.

In the model, the effects of TrkB activation and inhibition can be understood because of the threshold nature of eCB-STDP expression: eCB-tLTP is expressed when large amounts of 2-AG are produced and CB_1R is activated above the tLTP threshold (θ_{LTP}^{start}, Fig. 5D). In control conditions, CB_1R activation overcomes θ_{LTP}^{start} only for $N_{pairings}>6$ and up to $N_{pairings}<20$ (for larger $N_{pairings}$, CB_1R desensitization strongly reduces CB_1R activation), therefore eCB-tLTP is expressed for $6<N_{pairings}<20$ (Fig. 5C1). Part of the amount of 2-AG needed for CB_1R activation is contributed by TrkB via IP_3 production by PLCγ. For example, with ANA12, TrkB cannot be activated, which reduces the amount of IP_3 produced at each pairing and decreases production of 2-AG and activation of CB_1R compared to control conditions (Fig. D, *green*). 2-AG production with TrkB inhibited is not enough to overcome the LTP threshold, thus

explaining the disappearance of eCB-tLTP. The same reasoning explains that eCB-tLTD is considerably weakened under TrkB inhibition, as well as the effects of DHF.

Figure 5E1 shows the close agreement between model predictions and synaptic efficacy changes in control conditions and with the inhibition of TrkB (ANA12 conditions). In particular, under Trkb inhibition, the model faithfully reproduces the disappearance of eCB-tLTD at 100 pre-post pairings (shown experimentally in Figure 2) and that of eCB-tLTP at 10 post-pre pairings (shown experimentally in Figure 3).

The above results (Fig. 5C and E1) validate the model. We then used the model to derive experimentally-testable predictions about the effect of TrkB agonists (such as DHF). Figure 5E shows model prediction for the change of synaptic weight W with $N_{pairings}$ using STDP protocols yielding eCB-tLTP (upper curve, Δt=-20 ms) and eCB-tLTD (lower curve, Δt=+17ms). The model predicts that DHF should increase the amplitude of eCB-tLTP but also the range of $N_{pairings}$ values where it can be induced. The amplitude of eCB-tLTD should be increased, at least for $N_{pairings}$>25, with DHF (Fig. 5E2). Note that, in the model, the effects of TrkB are restricted to the activation of PLCγ and resulting changes in the production of IP_3 and DAG. The model does not integrate the other pathways of TrkB signaling (e.g. MAPK or PI3K). Therefore, experimental validation of the above predictions would strongly suggest that the effects of TrkB on eCB-STDP are mainly underlied by PLCγ.

Activation of TrkB promotes eCB-plasticity

We further investigated the causal role of TrkB activation in bidirectional eCB-plasticity and tested the model predictions (Fig. 5E). We tested two scenarios in which the boost in eCB synthesis operated by TrkB activation (with DHF, 10μM) should expand eCB-STDP domains for (*i*) eCB-tLTD (for $N_{pairings}$<50) and (*ii*) eCB-tLTP (for $N_{pairings}$>20). For this purpose, we chose two STDP protocols involving 25 pre-post and 25 post-pre pairings, for which eCB-tLTD

and eCB-tLTP, respectively, are not observed in control conditions (Cui et al., 2015; Cui et al., 2016).

First, we tested the effect of the activation of TrkB by DHF for 25 pre-post pairings. In control conditions, an absence of plasticity was observed following 25 pre-post pairings (99±3%, *p*=0.9728, n=6) (Fig. 6A). This result is in line with our previous reports showing that eCB-tLTD progressively disappeared when $N_{pairings}$<50 (Cui et al., 2015; Cui et al., 2016). Following DHF application, a tLTD was observed for 25 pre-post STDP pairings (61±5%, *p*=0.0001, n=7) (Fig. 6A and 6C). This tLTD was CB_1R-mediated since its expression was prevented by AM251 (3µM) (103±6%, *p*=0.6287, n=6) (Fig. 6B and 6C). Besides the PLCγ pathway, TrkB activation also leads to the recruitment of the MAPK and PI3K pathways. Thus, we next tested whether this DHF-induced eCBtLTD could still be induced following pharmacological blockade of the MAPK and PI3K pathways. For this purpose, specific inhibitors of MAP kinase kinases (MEK1 and MEK2), U0126 (10µM), and of PI3K, LY294002 (10µM), were co-applied during the whole experiment including STDP pairings. Under inhibition of the MAPK and PI3K pathways, DHF was still able to induce tLTD for 25 pre-post pairings (58±5%, *p*=0.0007, n=6) (Fig. 6B and 6C).

Second, we examined the effect of the activation of TrkB by DHF for the 25 post-pre STDP pairings. In control conditions, an absence of plasticity was observed after 25 post-pre pairings (101±5%, *p*=0.9238, n=7) (Fig. 6D). When we bath-applied DHF during the whole recording, no plasticity was induced after one hour (96±11%, *p*=0.7593, n=5) (Supplementary Fig. 3). We next restricted the application of DHF to the duration of the 25 STDP post-pre pairings. In these conditions, a reliable tLTP was observed (138±5%, *p*=0.0004, n=7) (Fig. 6D and 6F). This tLTP was CB_1R-dependent since its expression was prevented by AM251 (3µM) (102±4%, *p*=0.6951, n=5) (Fig. 6E and 6F). This eCB-tLTP did not involve the MAPK and PI3K pathways. Indeed, 25 post-pre pairings, with concomitant activation of TrkB (DHF

application), were still able to induce tLTP (148±6%, p=0.0014, n=5) even in presence of U0126 and LY294002 (Fig. 6E and 6F).

Therefore, eCB-plasticity appears to require the involvement of the PLCγ pathway following TrkB activation without the involvement of the MAPK and PI3K pathways.

In conclusion, these experiments confirm the model prediction that the activation of TrkB allows an enlargement of the domain of expression of eCB-tLTD and eCB–tLTP, indicating that TrkB efficiently gates but also shapes eCB-plasticity expression.

DISCUSSION

In the present study, we investigated the mechanistic and functional interaction between TrkB and eCB signaling in eCB-mediated LTD and LTP at corticostriatal synapses. We found that activation of TrkB is a necessary upstream modulator of eCB-dependent plasticity. Interestingly, this applied equally to distinct forms of corticostriatal plasticity induced by either rate-based (LFS) or spike-timing-based (STDP) paradigm. Here, we unveiled a novel mechanism by which BDNF shapes and gates corticostriatal plasticity. The corticostriatal axis is subjected to various forms of synaptic plasticity (Di Filippo et al., 2009; Surmeier et al., 2009; Lovinger, 2010). Long-term corticostriatal plasticity (LTP and LTD) provides a fundamental mechanism by which the basal ganglia encode action selection, goal directed behavior and habit formation (Yin et al., 2009; Koralek et al., 2012; Shan et al., 2014; Rothwell et al., 2015; Hawes et al., 2015; Xiong et al., 2015; Ma et al., 2018; Perrin and Venance, 2018). Importantly, the retrogradely acting eCBs have emerged as major players in learning and memory processes given their powerful influence in regulating corticostriatal plasticity (Lovinger, 2010; Mathur and Lovinger, 2012; Castillo et al., 2012; Araque et al., 2017). Synaptic plasticity is tightly controlled by various neuromodulators, also called the third factor (Foncelle et al., 2018), among which, BDNF appears to be indispensable for striatal functions (Baydyuk et al., 2011; Besusso et al., 2013; Unterwald et al., 2013). Indeed, in addition to its prominent role in inducing neuronal proliferation and differentiation, migration and survival, BDNF is a key regulator of synaptic transmission and plasticity in the adult brain (Carvalho et al., 2008; Waterhouse and Xu, 2009; Edelmann et al., 2014; Park et al., 2014). Intriguingly, compared to other neuronal networks where BDNF can act on both pre- and post-synaptic sites (Mohajerani et al., 2007; Sivakumaran et al, 2009; Inagaki et al., 2008; Edelmann et al., 2014), at the corticostriatal synapse BDNF is mainly released anterogradely and acts on postsynaptic TrkB (Baquet et al., 2004; Jia et al., 2010; Park et al., 2014). Such peculiarity is also supported

by the low contents of BDNF mRNA and the high levels of TrkB in MSNs (Altar et al., 1997; Conner et al., 1997; Freeman et al., 2003; Fumagalli et al., 2007; Berusso et al., 2013). Thus, eCBs and BDNF follow opposite ways of action in striatum, i.e. retrograde and anterograde, respectively. Nevertheless, these two systems establish cross-talks in various central structures (Khaspekov et al., 2004; Huang et al., 2008; Maison et al., 2009; Lemtiri-Chlieh and Levine 2010; Roloff et al., 2010; Luongo et al., 2014; Zhao et al. 2015; Zhong et al., 2015; Bennett et al., 2017; Yeh et al., 2017; Maglio et al., 2018). This is exemplified by the IPSC depression in layer 2/3 pyramidal neurons induced by BDNF-generated CB1R activation (Lemtiri-Chlieh and Levine, 2010; Zhao and Levine, 2014). Such effect involves an increase of PLC-dependent eCB release from pyramidal neurons, which ultimately leads to a decrease of GABA release from presynaptic inhibitory terminals (Lemtiri-Chlieh and Levine, 2010; Zhao and Levine, 2014) and results in inhibitory LTD (Zhao et al., 2015). Despites the characterization of multiple cross-talks between BDNF/TrkB and eCB systems (Bennett et al., 2017), the role of BDNF in eCB-mediated long-term plasticity has not been determined yet. We thus questioned the impact of BDNF in the striatum where various forms of bidirectional eCB-mediated plasticity occur (Cui et al. 2016; Araque et al., 2017; Xu et al., 2018).

Information in the brain can be engrammed via two main activity patterns : the rate- and spike-time coding (deCharms and Zador, 2000; Brette, 2015;), which can be mimicked experimentally by the use of two types of cell conditioning paradigms: rate-based and spike-timing-based protocols. Here, we show that BDNF regulates the expression of both rate- and spike-timing-based eCB-mediated long-term plasticity. Indeed, LFS-mediated LTD and bidirectional eCB-STDP are tightly dependent on the activation of TrkB. The common point of these LFS and STDP paradigms is that they were applied at 1 Hz presynaptic stimulation. This implies that BDNF might be efficiently released from cortical terminals at a low frequency, as recently observed in the hippocampus (Lu et al. 2014), and even for a low number of

stimulations, as exemplified for the eCB-tLTP which requires only 10 pairings. Interestingly, a recent study has shown that eCBs set the inhibition strength onto pyramidal cells of the barrel cortex, and in turn to calcium spike facilitation and to a form of BDNF-dependent LTP (Maglio et al., 2018). This report, together with our own results, suggests that the involvement of BDNF in eCB-plasticity is a paramount mechanism at various central synapses.

The effects of BDNF on synaptic plasticity are known to proceed via three major signaling pathways: PLCγ, MEK/ERK and PI3K/Akt (Patapoutian and Reichardt, 2001; Park and Poo, 2012; Edelmann et al, 2014). On the one hand, TrkB activation leads to the activation of PLCγ, which increases the levels of DAG and IP3. In turn this is expected to increase the production of 2-AG from DAG and to boost cytoplasmic calcium transients via IP3-dependent calcium release from internal stores. On the other hand, TrkB activates the MAPK/ERK and PI3K-Akt pathways, modulating plasticity through a range of potential mechanisms including AMPAR or NMDAR activity regulation. The PLCγ pathway, and the associated DAG and calcium boost upon TrkB activation, appears to be the best candidate for directly promoting eCB synthesis and release. It is well established that eCBs mobilization is promoted through transient increases in intracellular Ca^{2+} and activation of Gq-coupled receptors and subsequent PLC-dependent increase in DAG (Hashimotodani et al., 2007; Piomelli et al., 2007; Kano et al., 2009; Castillo, et al., 2012). BDNF is known to trigger local and fast transient increases in intracellular Ca^{2+} concentrations (Lang et al., 2007), an effect that has been attributed to slow mobilization of internal Ca^{2+} stores (Reichardt 2006; Amaral and Pozzo-Miller 2007) as well as to fast opening of voltage-gated Ca^{2+} channels (Kovalchuk et al., 2002). BDNF evokes transient calcium events in spines and dendrites of hippocampal granule cells and LTP is observed when these events are paired with weak synaptic stimulation (Kovalchuk et al., 2002). Using two-photon imaging combined with patch-clamp recordings in striatal MSNs, we show that TrkB activation modifies the kinetics of Ca^{2+} transients triggered by bAPs only, pre-post

or post-pre STDP pairings. Indeed, TrkB activation promotes longer Ca^{2+} transients (this effect was prevented by TrkB antagonist), yielding a larger quantity of intracellular Ca^{2+} and potentially a larger eCB synthesis and release. Interestingly, we observed these modifications of Ca^{2+} transients in spines but not in dendritic shafts.

In addition, to determine which pathway was required for TrkB-induced eCB-STDP (PLCγ, MAPK/ERK and/or PI3K-Akt pathways), we assembled a mathematical model describing the temporal dynamics of the biochemical reactions implicated in corticostriatal synaptic plasticity. The model accounted for the PLCγ pathway, disregarding the MAPK and PI3K-Akt pathways. Supporting this option, we showed that when MAPK and PI3K-Akt pathways were blocked, eCB-STDP could still be observed (Fig. 6), demonstrating that MAPK and PI3K-Akt pathways are not required for eCB-mediated plasticity at corticostriatal synapses. Beyond the very good match with the experimental data, the model predicted that TrkB agonists would facilitate the expression of eCB-tLTP and to a lesser extent of eCB-tLTD. Experimental validation of this prediction is a strong indication that TrkB modulation of eCB-tLTP proceeds via PLCγ, not MAPK nor PI3K. Namely, it was possible to enlarge the domains of expression of eCB-tLTP and eCB-tLTD by acting directly on TrkB activation as predicted by the mathematical model. Indeed, for pairings that did not induce eCB-tLTP and eCB-tLTD in control conditions, i.e. 25 post-pre and 25 pre-post pairings, respectively, (Cui et al., 2015; Cui et al., 2016; Xu et al., 2018), the activation of TrkB allows a considerable remodeling of the domain of expression of eCB-plasticity: when TrkB was activated by DHF during the 25 post-pre pairings, an eCB-dependent tLTP could be induced. Note however that, when DHF was applied all along the recording (ie the 25 post-pre pairings plus the following hour of recording) no plasticity was observed. These results may indicate that a brief and transient activation of TrkB is required for tLTP, whereas prolonged activation of TrkB would lead to tLTD. This is in line with the mechanisms that promote eCB-tLTD and eCB-tLTP: moderate levels and prolonged releases

of eCBs lead to tLTD, whereas brief releases of large eCB concentration yield tLTP (Cui et al., 2016; Cui et al., 2018; Xu et al., 2018). This indicates that the temporal activation of TrkB is essential not only for the expression of eCB-STDP but also for its expression domains, in a way similar to eCBs (Cui et al., 2016). It is not currently possible to specifically block PLCγ activity because of the absence of a selective inhibitor that would exclusively target the γ isoform leaving the others (mostly β and δ) unaffected. The use of unspecific PLC antagonists (such as the widely-used U-73122) would prevent the synthesis of eCB by inhibiting PLCβ, a key actor in 2-AG production (Castillo et al., 2012; Hashimotodani et al., 2007). Therefore, we opted for the strategy of blocking the MAPK and PI3K pathways and examine whether eCB-plasticity would be affected. We found that blocking specifically both the MAPK and PI3K pathways does not abrogate TrkB-mediated eCB-tLTD and eCB-tLTP. Experimental evidence and model results therefore converge to strongly suggests that the modulation of eCB-STDP by TrkB specifically acts via the PLCγ pathway, not the MAPK nor PI3K.

In neurodegenerative diseases, such as Huntington disease, (Strand et al. 2007; Zuccato and Cattaneo 2009; Park 2018; Yu et al. 2018) and neurodevelopmental disorders (Autry and Monteggia 2012; Baydyuk and Xu 2014; Deinhardt and Chao 2014), BDNF release is strongly diminished. In the light of our results, this reduction of BDNF account for the reduction or the loss of synaptic plasticity, as observed in Huntington disease rodent models (Kolodziejczyk et al. 2014; Plotkin et al. 2014; Sepers et al. 2018). On the opposite, BDNF levels are increased in maladaptive disorders such as ethanol or cocaine addiction (Jeanblanc et al. 2009; Im et al. 2010; Lu et al. 2010; Bahi and Dreyer 2013). In these cases, some aberrant plasticity has been observed (Deinhardt and Chao 2014; Zlebnik and Cheer 2016) in line with our results showing that an over-activation of TrkB triggers a remodeling and an enlargement of the domains of expression of Hebbian plasticity. In conclusion our study unveils a novel synaptic mechanism by which BDNF/TrkB governs striatal functions, thus potentially paving the way to a better

understanding of a range of diseases in which alteration or disruption of BDNF/TrkB signaling has been recognized as causative feature for learning and memory deficits.

ACKNOWLEDGMENTS

We thank the L.V. lab members for helpful suggestions and critical comments. This work was supported by grants from Fondation Patrick Brou de Laurière, INSERM, INRIA, Collège de France and CNRS. G.G is supported by by Fondation Patrick Brou de Laurière.

REFERENCES

Alger BE, Kim J. 2011. Supply and demand for endocannabinoids. Trends Neurosci. 34:304–315.

Altar CA, Cai N, Bliven T, Juhasz M, Conner JM, Acheson AL, Lindsay RM, Wiegand SJ. 1997. Anterograde transport of brain-derived neurotrophic factor and its role in the brain. Nature. 389:856–860.

Amaral MD, Pozzo-Miller L. 2007. TRPC3 channels are necessary for brain-derived neurotrophic factor to activate a nonselective cationic current and to induce dendritic spine formation. J Neurosci. 27:5179–5189.

Araque A, Castillo PE, Manzoni OJ, Tonini R. 2017. Synaptic functions of endocannabinoid signaling in health and disease. Neuropharmacology. 124:13–24.

Autry AE, Monteggia LM. 2012. Brain-derived neurotrophic factor and neuropsychiatric disorders. Pharmacol Rev. 64:238–258.

Bahi A, Dreyer J-L. 2013. Striatal modulation of BDNF expression using microRNA124a-expressing lentiviral vectors impairs ethanol-induced conditioned-place preference and voluntary alcohol consumption. Eur J Neurosci. 38:2328–2337.

Baquet ZC, Gorski JA, Jones KR. 2004. Early striatal dendrite deficits followed by neuron loss with advanced age in the absence of anterograde cortical brain-derived neurotrophic factor. J Neurosci. 24:4250–4258.

Baydyuk M, Russell T, Liao G-Y, Zang K, An JJ, Reichardt LF, Xu B. 2011. TrkB receptor controls striatal formation by regulating the number of newborn striatal neurons. Proc Natl Acad Sci USA. 108:1669–1674.

Baydyuk M, Xu B. 2014. BDNF signaling and survival of striatal neurons. Front Cell Neurosci. 8:254.

Bennett MR, Arnold J, Hatton SN, Lagopoulos J. 2017. Regulation of fear extinction by long-term depression: The roles of endocannabinoids and brain derived neurotrophic factor. Behav Brain Res. 319:148–164.

Besusso D, Geibel M, Kramer D, Schneider T, Pendolino V, Picconi B, Calabresi P, Bannerman DM, Minichiello L. 2013. BDNF-TrkB signaling in striatopallidal neurons controls inhibition of locomotor behavior. Nat Commun. 4:2031.

Brette R. 2015. Philosophy of the Spike: Rate-Based vs. Spike-Based Theories of the Brain. Front Syst Neurosci. 9:151.

Carvalho AL, Caldeira MV, Santos SD, Duarte CB. 2008. Role of the brain-derived neurotrophic factor at glutamatergic synapses. Br J Pharmacol. 153 Suppl 1:S310-324.

Castillo PE, Younts TJ, Chávez AE, Hashimotodani Y. 2012. Endocannabinoid signaling and synaptic function. Neuron. 76:70–81.

Chevaleyre V, Takahashi KA, Castillo PE. 2006. Endocannabinoid-mediated synaptic plasticity in the CNS. Annu Rev Neurosci. 29:37–76.

Conner JM, Lauterborn JC, Yan Q, Gall CM, Varon S. 1997. Distribution of brain-derived neurotrophic factor (BDNF) protein and mRNA in the normal adult rat CNS: evidence for anterograde axonal transport. J Neurosci. 17:2295–2313.

Cui Y, Paillé V, Xu H, Genet S, Delord B, Fino E, Berry H, Venance L. 2015. Endocannabinoids mediate bidirectional striatal spike-timing-dependent plasticity. J Physiol (Lond). 593:2833–2849.

Cui Y, Prokin I, Mendes A, Berry H, Venance L. 2018. Robustness of STDP to spike timing jitter. Sci Rep. 8:8139.

Cui Y, Prokin I, Xu H, Delord B, Genet S, Venance L, Berry H. 2016. Endocannabinoid dynamics gate spike-timing dependent depression and potentiation. Elife. 5:e13185.

deCharms RC, Zador A. 2000. Neural representation and the cortical code. Annu Rev Neurosci. 23:613–647.
Deinhardt K, Chao MV. 2014. Shaping neurons: Long and short range effects of mature and proBDNF signalling upon neuronal structure. Neuropharmacology. 76 Pt C:603–609.
Di Filippo M, Picconi B, Tantucci M, Ghiglieri V, Bagetta V, Sgobio C, Tozzi A, Parnetti L, Calabresi P. 2009. Short-term and long-term plasticity at corticostriatal synapses: implications for learning and memory. Behav Brain Res. 199:108–118.
Di Marzo V. 2008. Targeting the endocannabinoid system: to enhance or reduce? Nat Rev Drug Discov. 7:438–455.
Edelmann E, Lessmann V, Brigadski T. 2014. Pre- and postsynaptic twists in BDNF secretion and action in synaptic plasticity. Neuropharmacology. 76 Pt C:610–627.
Eldeeb K, Leone-Kabler S, Howlett AC. 2016. CB1 cannabinoid receptor-mediated increases in cyclic AMP accumulation are correlated with reduced Gi/o function. J Basic Clin Physiol Pharmacol. 27:311–322.
Fino E, Glowinski J, Venance L. 2005. Bidirectional activity-dependent plasticity at corticostriatal synapses. J Neurosci. 25:11279–11287.
Fino E, Paille V, Cui Y, Morera-Herreras T, Deniau J-M, Venance L. 2010. Distinct coincidence detectors govern the corticostriatal spike timing-dependent plasticity. J Physiol (Lond). 588:3045–3062.
Foncelle A, Mendes A, Jędrzejewska-Szmek J, Valtcheva S, Berry H, Blackwell KT, Venance L. 2018. Modulation of Spike-Timing Dependent Plasticity: Towards the Inclusion of a Third Factor in Computational Models. Front Comput Neurosci. 12:49.
Freeman AY, Soghomonian J-J, Pierce RC. 2003. Tyrosine kinase B and C receptors in the neostriatum and nucleus accumbens are co-localized in enkephalin-positive and enkephalin-negative neuronal profiles and their expression is influenced by cocaine. Neuroscience. 117:147–156.
Fumagalli F, Di Pasquale L, Caffino L, Racagni G, Riva MA. 2007. Repeated exposure to cocaine differently modulates BDNF mRNA and protein levels in rat striatum and prefrontal cortex. Eur J Neurosci. 26:2756–2763.
Glass M, Felder CC. 1997. Concurrent stimulation of cannabinoid CB1 and dopamine D2 receptors augments cAMP accumulation in striatal neurons: evidence for a Gs linkage to the CB1 receptor. J Neurosci. 17:5327–5333.
Graybiel AM, Grafton ST. 2015. The striatum: where skills and habits meet. Cold Spring Harb Perspect Biol. 7:a021691.
Hashimotodani Y, Ohno-Shosaku T, Tsubokawa H, Ogata H, Emoto K, Maejima T, Araishi K, Shin H-S, Kano M. 2005. Phospholipase Cbeta serves as a coincidence detector through its Ca2+ dependency for triggering retrograde endocannabinoid signal. Neuron. 45:257–268.
Hashimotodani Y, Ohno-Shosaku T, Watanabe M, Kano M. 2007. Roles of phospholipase Cbeta and NMDA receptor in activity-dependent endocannabinoid release. J Physiol (Lond). 584:373–380.
Hawes SL, Evans RC, Unruh BA, Benkert EE, Gillani F, Dumas TC, Blackwell KT. 2015. Multimodal Plasticity in Dorsal Striatum While Learning a Lateralized Navigation Task. J Neurosci. 35:10535–10549.
Heifets BD, Castillo PE. 2009. Endocannabinoid signaling and long-term synaptic plasticity. Annu Rev Physiol. 71:283–306.
Huang Y, Yasuda H, Sarihi A, Tsumoto T. 2008. Roles of endocannabinoids in heterosynaptic long-term depression of excitatory synaptic transmission in visual cortex of young mice. J Neurosci. 28:7074–7083.

Im H-I, Hollander JA, Bali P, Kenny PJ. 2010. MeCP2 controls BDNF expression and cocaine intake through homeostatic interactions with microRNA-212. Nat Neurosci. 13:1120–1127.

Inagaki T, Begum T, Reza F, Horibe S, Inaba M, Yoshimura Y, Komatsu Y. 2008. Brain-derived neurotrophic factor-mediated retrograde signaling required for the induction of long-term potentiation at inhibitory synapses of visual cortical pyramidal neurons. Neurosci Res. 61:192–200.

Jarrahian A, Watts VJ, Barker EL. 2004. D2 dopamine receptors modulate Galpha-subunit coupling of the CB1 cannabinoid receptor. J Pharmacol Exp Ther. 308:880–886.

Jeanblanc J, He D-Y, Carnicella S, Kharazia V, Janak PH, Ron D. 2009. Endogenous BDNF in the dorsolateral striatum gates alcohol drinking. J Neurosci. 29:13494–13502.

Jia Y, Gall CM, Lynch G. 2010. Presynaptic BDNF promotes postsynaptic long-term potentiation in the dorsal striatum. J Neurosci. 30:14440–14445.

Jing D, Lee FS, Ninan I. 2017. The BDNF Val66Met polymorphism enhances glutamatergic transmission but diminishes activity-dependent synaptic plasticity in the dorsolateral striatum. Neuropharmacology. 112:84–93.

Kano M, Ohno-Shosaku T, Hashimotodani Y, Uchigashima M, Watanabe M. 2009. Endocannabinoid-mediated control of synaptic transmission. Physiol Rev. 89:309–380.

Kearn CS, Blake-Palmer K, Daniel E, Mackie K, Glass M. 2005. Concurrent stimulation of cannabinoid CB1 and dopamine D2 receptors enhances heterodimer formation: a mechanism for receptor cross-talk? Mol Pharmacol. 67:1697–1704.

Khaspekov LG, Brenz Verca MS, Frumkina LE, Hermann H, Marsicano G, Lutz B. 2004. Involvement of brain-derived neurotrophic factor in cannabinoid receptor-dependent protection against excitotoxicity. Eur J Neurosci. 19:1691–1698.

Kolodziejczyk K, Parsons MP, Southwell AL, Hayden MR, Raymond LA. 2014. Striatal synaptic dysfunction and hippocampal plasticity deficits in the Hu97/18 mouse model of Huntington disease. PLoS ONE. 9:e94562.

Koralek AC, Jin X, Long JD, Costa RM, Carmena JM. 2012. Corticostriatal plasticity is necessary for learning intentional neuroprosthetic skills. Nature. 483:331–335.

Kovalchuk Y, Hanse E, Kafitz KW, Konnerth A. 2002. Postsynaptic Induction of BDNF-Mediated Long-Term Potentiation. Science. 295:1729–1734.

Lang SB, Stein V, Bonhoeffer T, Lohmann C. 2007. Endogenous brain-derived neurotrophic factor triggers fast calcium transients at synapses in developing dendrites. J Neurosci. 27:1097–1105.

Lemtiri-Chlieh F, Levine ES. 2010. BDNF evokes release of endogenous cannabinoids at layer 2/3 inhibitory synapses in the neocortex. J Neurophysiol. 104:1923–1932.

Lovinger DM. 2010. Neurotransmitter roles in synaptic modulation, plasticity and learning in the dorsal striatum. Neuropharmacology. 58:951–961.

Lu H, Cheng P-L, Lim BK, Khoshnevisrad N, Poo M-M. 2010. Elevated BDNF after cocaine withdrawal facilitates LTP in medial prefrontal cortex by suppressing GABA inhibition. Neuron. 67:821–833.

Lu H, Park H, Poo M-M. 2014. Spike-timing-dependent BDNF secretion and synaptic plasticity. Philos Trans R Soc Lond, B, Biol Sci. 369:20130132.

Luongo L, Maione S, Di Marzo V. 2014. Endocannabinoids and neuropathic pain: focus on neuron-glia and endocannabinoid-neurotrophin interactions. Eur J Neurosci. 39:401–408.

Ma T, Cheng Y, Roltsch Hellard E, Wang X, Lu J, Gao X, Huang CCY, Wei X-Y, Ji J-Y, Wang J. 2018. Bidirectional and long-lasting control of alcohol-seeking behavior by corticostriatal LTP and LTD. Nat Neurosci. 21:373–383.

Maglio LE, Noriega-Prieto JA, Maraver MJ, Fernández de Sevilla D. 2018. Endocannabinoid-Dependent Long-Term Potentiation of Synaptic Transmission at Rat Barrel Cortex. Cereb Cortex. 28:1568–1581.
Maison P, Walker DJ, Walsh FS, Williams G, Doherty P. 2009. BDNF regulates neuronal sensitivity to endocannabinoids. Neurosci Lett. 467:90–94.
Mathur BN, Lovinger DM. 2012. Endocannabinoid-dopamine interactions in striatal synaptic plasticity. Front Pharmacol. 3:66.
Mohajerani MH, Sivakumaran S, Zacchi P, Aguilera P, Cherubini E. 2007. Correlated network activity enhances synaptic efficacy via BDNF and the ERK pathway at immature CA3 CA1 connections in the hippocampus. Proc Natl Acad Sci USA. 104:13176–13181.
Paille V, Fino E, Du K, Morera-Herreras T, Perez S, Kotaleski JH, Venance L. 2013. GABAergic circuits control spike-timing-dependent plasticity. J Neurosci. 33:9353–9363.
Park H. 2018. Cortical Axonal Secretion of BDNF in the Striatum Is Disrupted in the Mutant-huntingtin Knock-in Mouse Model of Huntington's Disease. Exp Neurobiol. 27:217–225.
Park H, Poo M. 2013. Neurotrophin regulation of neural circuit development and function. Nat Rev Neurosci. 14:7–23.
Park H, Popescu A, Poo M. 2014. Essential role of presynaptic NMDA receptors in activity-dependent BDNF secretion and corticostriatal LTP. Neuron. 84:1009–1022.
Patapoutian A, Reichardt LF. 2001. Trk receptors: mediators of neurotrophin action. Curr Opin Neurobiol. 11:272–280.
Pawlak V, Kerr JND. 2008. Dopamine receptor activation is required for corticostriatal spike-timing-dependent plasticity. J Neurosci. 28:2435–2446.
Perrin E, Venance L. 2019. Bridging the gap between striatal plasticity and learning. Curr Opin Neurobiol. 54:104–112.
Piomelli D. 2003. The molecular logic of endocannabinoid signalling. Nat Rev Neurosci. 4:873–884.
Piomelli D, Astarita G, Rapaka R. 2007. A neuroscientist's guide to lipidomics. Nat Rev Neurosci. 8:743–754.
Plotkin JL, Day M, Peterson JD, Xie Z, Kress GJ, Rafalovich I, Kondapalli J, Gertler TS, Flajolet M, Greengard P, Stavarache M, Kaplitt MG, Rosinski J, Chan CS, Surmeier DJ. 2014. Impaired TrkB receptor signaling underlies corticostriatal dysfunction in Huntington's disease. Neuron. 83:178–188.
Puente N, Cui Y, Lassalle O, Lafourcade M, Georges F, Venance L, Grandes P, Manzoni OJ. 2011. Polymodal activation of the endocannabinoid system in the extended amygdala. Nat Neurosci. 14:1542–1547.
Reichardt LF. 2006. Neurotrophin-regulated signalling pathways. Philos Trans R Soc Lond, B, Biol Sci. 361:1545–1564.
Roloff AM, Anderson GR, Martemyanov KA, Thayer SA. 2010. Homer 1a gates the induction mechanism for endocannabinoid-mediated synaptic plasticity. J Neurosci. 30:3072–3081.
Rothwell PE, Hayton SJ, Sun GL, Fuccillo MV, Lim BK, Malenka RC. 2015. Input- and Output-Specific Regulation of Serial Order Performance by Corticostriatal Circuits. Neuron. 88:345–356.
Schulz JM, Redgrave P, Reynolds JNJ. 2010. Cortico-striatal spike-timing dependent plasticity after activation of subcortical pathways. Front Synaptic Neurosci. 2:23.
Sepers MD, Smith-Dijak A, LeDue J, Kolodziejczyk K, Mackie K, Raymond LA. 2018. Endocannabinoid-Specific Impairment in Synaptic Plasticity in Striatum of Huntington's Disease Mouse Model. J Neurosci. 38:544–554.

Shan Q, Ge M, Christie MJ, Balleine BW. 2014. The acquisition of goal-directed actions generates opposing plasticity in direct and indirect pathways in dorsomedial striatum. J Neurosci. 34:9196–9201.

Shen X, Lin X, De Wilde P. 2008. Oscillations and spiking pairs: behavior of a neuronal model with STDP learning. Neural Comput. 20:2037–2069.

Sivakumaran S, Mohajerani MH, Cherubini E. 2009. At immature mossy-fiber-CA3 synapses, correlated presynaptic and postsynaptic activity persistently enhances GABA release and network excitability via BDNF and cAMP-dependent PKA. J Neurosci. 29:2637–2647.

Strand AD, Baquet ZC, Aragaki AK, Holmans P, Yang L, Cleren C, Beal MF, Jones L, Kooperberg C, Olson JM, Jones KR. 2007. Expression profiling of Huntington's disease models suggests that brain-derived neurotrophic factor depletion plays a major role in striatal degeneration. J Neurosci. 27:11758–11768.

Surmeier DJ, Plotkin J, Shen W. 2009. Dopamine and synaptic plasticity in dorsal striatal circuits controlling action selection. Curr Opin Neurobiol. 19:621–628.

Unterwald EM, Page ME, Brown TB, Miller JS, Ruiz M, Pescatore KA, Xu B, Reichardt LF, Beverley J, Tang B, Steiner H, Thomas EA, Ehrlich ME. 2013. Behavioral and transcriptome alterations in male and female mice with postnatal deletion of TrkB in dorsal striatal medium spiny neurons. Mol Neurodegener. 8:47.

Valtcheva S, Paillé V, Dembitskaya Y, Perez S, Gangarossa G, Fino E, Venance L. 2017. Developmental control of spike-timing-dependent plasticity by tonic GABAergic signaling in striatum. Neuropharmacology. 121:261–277.

Waterhouse EG, Xu B. 2009. New insights into the role of brain-derived neurotrophic factor in synaptic plasticity. Mol Cell Neurosci. 42:81–89.

Xiong Q, Znamenskiy P, Zador AM. 2015. Selective corticostriatal plasticity during acquisition of an auditory discrimination task. Nature. 521:348–351.

Xu H, Perez S, Cornil A, Detraux B, Prokin I, Cui Y, Degos B, Berry H, de Kerchove d'Exaerde A, Venance L. 2018. Dopamine-endocannabinoid interactions mediate spike-timing-dependent potentiation in the striatum. Nat Commun. 9:4118.

Yeh ML, Selvam R, Levine ES. 2017. BDNF-induced endocannabinoid release modulates neocortical glutamatergic neurotransmission. Synapse. 71.

Yin HH, Knowlton BJ. 2006. The role of the basal ganglia in habit formation. Nat Rev Neurosci. 7:464–476.

Yin HH, Mulcare SP, Hilário MRF, Clouse E, Holloway T, Davis MI, Hansson AC, Lovinger DM, Costa RM. 2009. Dynamic reorganization of striatal circuits during the acquisition and consolidation of a skill. Nat Neurosci. 12:333–341.

Yu C, Li CH, Chen S, Yoo H, Qin X, Park H. 2018. Decreased BDNF Release in Cortical Neurons of a Knock-in Mouse Model of Huntington's Disease. Sci Rep. 8:16976.

Zhao L, Levine ES. 2014. BDNF-endocannabinoid interactions at neocortical inhibitory synapses require phospholipase C signaling. J Neurophysiol. 111:1008–1015.

Zhao L, Yeh ML-W, Levine ES. 2015. Role for Endogenous BDNF in Endocannabinoid-Mediated Long-Term Depression at Neocortical Inhibitory Synapses. eNeuro. 2.

Zhong P, Liu Y, Hu Y, Wang T, Zhao Y, Liu Q. 2015. BDNF interacts with endocannabinoids to regulate cocaine-induced synaptic plasticity in mouse midbrain dopamine neurons. J Neurosci. 35:4469–4481.

Zlebnik NE, Cheer JF. 2016. Drug-Induced Alterations of Endocannabinoid-Mediated Plasticity in Brain Reward Regions. J Neurosci. 36:10230–10238.

Zuccato C, Cattaneo E. 2009. Brain-derived neurotrophic factor in neurodegenerative diseases. Nat Rev Neurol. 5:311–322.

CAPTIONS TO FIGURES

Figure 1: eCB-LTD induced with LFS relies on TrkB activation

(**A**) Scheme of the recording and stimulating sites in cortico-striatal horizontal slices and LFS protocol. (**B**) LFS protocol: 600 cortical stimulations at 1 Hz were paired with concomitant postsynaptic subthreshold depolarizations. (**C-D**) Corticostriatal eCB-mediated LTD induced by LFS. (**C**) Example of LTD induced by LFS the mean baseline EPSC amplitude was 268±4pA before LFS and decreased by 60% to 106±1pA one hour after LFS protocol (p=0.0001). Bottom, time course of Ri (baseline: 109±0.4MΩ and 50-60 min after pairings: 106±1MΩ; change of 3.6%) for this cell. (**D**) Averaged time-courses of LTD induced by LFS (7/7 cells showed LTD); this LFS-LTD was dependent on CB_1R activation, because AM251 (3 μM) prevented tLTD (2/6 cells showed LTD). (**E-G**) Corticostriatal LFS-LTD relies on TrkB activation. (**E**) Example of the lack of LTD after LFS in presence of K252a (200 nM) (240±4pA before LFS and a lack of plasticity was observed one hour after LFS: 254±6pA, *p*=0.0561). Bottom, time course of Ri (baseline: 75±1MΩ and 50-60 min after pairings: 74±0.2MΩ; change of 1.4%). (**F**) Averaged time-courses showing the lack of LTD after LFS in presence of K252a (3/8 cells showed LTD) or with ANA12 (3/9 cells showed LTD). (**G**) Example of the lack of LTD after LFS in presence of ANA12 (10 μM) (286±11pA before LFS and 310±5pA one hour after LFS, *p*=0.0735). Bottom, time course of Ri (baseline: 98±1MΩ and 50-60 min after pairings: 93±1MΩ; change of 5%). (**H**) Graph bars of the averaged responses for all control, AM251, K252a and ANA12 conditions (One-way ANOVA, $F_{(3,26)} = 7.784$; p = 0.0007).

Insets (in **D** and **F**) correspond to the average EPSC amplitude during baseline (black trace) and during the last 10 min of recordings after LFS (grey trace). Error bars represent the SEM. ***: *p*<0.001; ns: not significant.

Figure 2: eCB-tLTD relies on TrkB activation

(**A**) Scheme of the recording and stimulating sites in corticostriatal horizontal slices and the STDP protocol: a single cortical stimulation was paired with a single spike evoked by a depolarizing current step in the recorded striatal MSN, in a pre-post sequence ($0<\Delta t_{STDP}<+20$ ms); this pairing was repeated 100 times at 1 Hz. (**B**) Corticostriatal eCB-mediated tLTD. Averaged time-courses of tLTD induced by 100 pre-post pairings (8/10 cells displayed tLTD); this tLTD was mediated by CB_1R, because tLTD was prevented by the application of AM251 (3 µM) (1/5 cells showed tLTD). (**C**) Corticostriatal eCB-tLTD relies on TrkB activation. Averaged time-courses showing the lack of plasticity observed with K252a (1/9 showed tLTD) and with ANA12 (3/10 showed LTD). (**D**) Graph bars of the averaged responses for all control, AM251, K252a and ANA12 conditions (One-way ANOVA, $F_{(3,30)} = 4.84$; $p = 0.0073$).

Insets (**B** and **C**) correspond to the average EPSC amplitude during baseline (black trace) and during the last 10 min of recording after STDP pairings (grey trace). Error bars represent the SEM. **: $p<0.01$; ns: not significant.

Figure 3: eCB-tLTP relies on TrkB activation

(**A**) Scheme of the recording and stimulating sites in cortico-striatal horizontal slices and the STDP protocol: a single cortical stimulation was paired with a single spike evoked by a depolarizing current step in the recorded striatal MSN, in a post-pre sequence ($-20<\Delta t_{STDP}<0$ ms); this pairing was repeated 10 times at 1 Hz. (**B**) Corticostriatal eCB-mediated tLTP. Averaged time-courses of tLTP induced by 10 post-pre pairings (6/9 cells showed tLTP); this tLTP was mediated by CB_1R, because tLTP was prevented by the application of AM251 (3 µM) (0/6 showed tLTP). (**C**) Corticostriatal eCB-tLTP relies on TrkB activation. Averaged time-courses showing the lack of plasticity observed with K252a (0/10 showed tLTP, and 8/10 showed tLTD) or with ANA12 (0/7 showed tLTP). (**D**) Graph bars of the averaged responses

for all control, AM251, K252a and ANA12 conditions (One-way ANOVA, $F_{(3,28)} = 8.60$; p = 0.0003).

Insets (**B** and **C**) correspond to the average EPSC amplitude during baseline (black trace) and during the last 10 min of recording after STDP pairings (grey trace). Error bars represent the SEM. ***: $p<0.001$; ns: not significant.

Figure 4: Activation of TrkB boosts calcium transients in dendritic spines

(**A**) (**A1**) experimental set-up showing the combination of whole-cell patch-clamp of a single MSN (see the patch-clamp pipette underlined in white) with two-photon imaging; the dashed white square indicated the imaged area). The scanning areas had been selected on 100-150 µm distance from soma. (**A2**) Line-scanning two-photon microscopy of Ca^{2+} transients in dendritic spines and adjacent shafts in MSNs filled with (**A3**) ratiometric indicators Fluo-4F (250 µM) and Alexa Fluor 594 (50 µM). (**B-D**) DHF increased Ca^{2+} transients in dendritic spines, but not in shafts, triggered by (**B**) two bAPs (post-stimulation only), (**C**) paired stimulation, consisting in single evoked corticostriatal EPSP paired with two bAPs with Δt ~+15-20 ms, or (**D**) paired stimulation, consisting two bAPs paired with single evoked corticostriatal EPSP with Δt ~-15-20 ms.

Error bars represent the SEM. *: $p<0.05$; **: $p<0.01$; ns: not significant.

Figure 5: Effects of TrkB agonists in a mathematical model of the signaling pathways

(**A**) Scheme of the main signaling pathways accounted for in the mathematical model. The model expresses the kinetics of the corresponding enzymatic and binding reactions. To derive it, we used the mathematical model for corticostriatal STDP (Cui et al, 2016; Cui et al., 2018) and added the production of IP3 and DAG by TrkB-activated PLCγ. The full grey circles located the reactions that are controlled by cytosolic Ca^{2+}. The synaptic weight W is defined by

$W_{total=}W_{post}\times W_{pre}$. Abbreviations: CICR: Ca^{2+}-induced Ca^{2+}-release, mGluR: metabotropic glutamate receptor, AEA: anandamide; VSCC: Voltage-Sensitive Ca^{2+}channels; TRPV1: Transient Receptor Potential cation channel subfamily V type 1. (**B**) Effect of the activation of TrkB and inhibition of TrkB on transients of cytosolic Ca^{2+} triggered by a single postsynaptic stimulation (to be compared with the experimental traces obtained in Fig. 4B). (**C**) Changes of the synaptic weight *W* in the model when the spike timing Δt_{STDP} and the number of pairings of the STDP protocol are varied. *W* is analyzed in control conditions (**C1**), with TrkB activated (such as DHF-like conditions) (**C2**), and with TrkB inhibited (such as ANA12- or K252a-like conditions) (**C3**). The colorcode for those maps is given at the end of the line. (**D**) Time course of the model prediction for the activation of CB_1Rs during the first 10 paired stimulations in control conditions (*blue*) and with activation of TrkB (*red*) or inhibition of TrkB (*green*). According to the model, tLTP is expressed when CB_1R activation overcomes the threshold θ_{LTP}^{start}, whereas tLTD is expressed when CB_1R activation is between θ_{LTD}^{start} and θ_{LTD}^{stop}. Δt_{STDP}=-15 ms. (**E1**) Comparison of the effects of an inhibition of TrkB in the model (*blue*) with the experimental results (data with ANA12) (*orange*). (**E2**) Model predictions for the effects of the activation of TrkB on the changes of *W* with $N_{pairings}$. In **E1** and **E2**, simulation for the model were performed for 100 pre-post pairings at Δt_{STDP}=+17 ms and for 10 post-pre pairings at Δt_{STDP}= -20 ms

Figure 6: Activation of TrkB promotes eCB-plasticity

(**A**) Activation of TrkB with DHF (10μM) promotes eCB-tLTD for 25 pre-post pairings. Averaged time-courses showing the absence of plasticity (1/6 showed tLTD) in control conditions, and tLTD induced by 25 pre-post pairings with DHF bath-applied during STDP pairings (7/7 showed tLTD). (**B**) This tLTD was mediated by CB_1R, because it was prevented by the application of AM251 (3μM) (0/6 showed tLTD). Inhibition of MAPK and PI3K

pathways with U0126 (10μM) and LY294002 (10μM) did not prevent tLTD induced by 25 pre-post pairings with DHF (6/6 showed tLTD). (**C**) Summary bar graphs showing the eCB-tLTD induced by DHF together with 25 pre-post pairings and which is independent of the MAPK and PI3K pathways (One-way ANOVA, $F_{(3,21)} = 32.44$; $p = 0.0001$).

(**D**) DHF promotes eCB-tLTP for 25 post-pre pairings. Averaged time-courses showing the absence of plasticity (3/7 showed tLTP) observed after 25 pre-post pairings in control conditions, and tLTP induced by 25 post-pre pairings with DHF bath-applied during STDP pairings (7/7 showed tLTP). (**E**) this tLTP was mediated by CB_1R, because it was prevented by AM251 (1/5 showed tLTP). Inhibition of MAPK and PI3K pathways with U0126 (10μM) and LY294002 (10μM) did not prevent tLTP induced by 25 post-pre pairings with DHF (5/5 showed tLTP). (**F**) Summary bar graphs showing the eCB-tLTP induced by DHF together with 25 post-pre pairings and which is independent of the MAPK and PI3K pathways (One-way ANOVA, $F_{(3,20)} = 18.16$; $p = 0.0001$).

Insets correspond to the average EPSC amplitude during baseline (black trace) and the last 10 min of recording after STDP pairings (grey trace). Error bars represent the SEM. ***: $p<0.001$; ns: not significant.

SUPPLEMENTARY MATERIAL

Legends of the Supplementary Figures:

Supplementary Figure 1: Representative STDP experiments (related the main Figures 2 and 3).

(A) Example of tLTD induced by 100 pre-post pairings (Δt_{STDP}=-13±0.1ms) (baseline: 159±5pA, decreased by 56.7%, to 69±3pA, one hour after pairings.). Bottom, time course of Ri (baseline: 104.3±0.38 MΩ and 50-60 min after pairings: 111±0.4MΩ; change of 5.9%). (**B**) Example of the lack of plasticity after 100 pre-post pairings (Δt_{STDP}=8±0.1ms) with K252a (200nM) (the mean baseline EPSC amplitude was 119.2±2.62 pA before pairings and a lack of plasticity was observed one hour after pairings: 117.6±2.99 pA). Bottom, time course of Ri (baseline: 213±1MΩ and 50-60 min after pairings: 209±2MΩ; change of 1.8%). (**C**) Example of the lack of plasticity after 100 pre-post pairings (Δt_{STDP}=13±0.1ms) in presence of ANA12 (10μM) (the mean baseline EPSC amplitude was 187.2±3.73 pA before pairings and was not significantly altered one hour after pairings, 184.4±3.32 pA). Bottom, time course of Ri (baseline: 107±1MΩ and 50-60 min after pairings: 109±0.5MΩ; change of 2%).

(**D**) Example of tLTP induced by 10 post-pre pairings (Δt_{STDP}=-11±0.1ms) (the mean baseline EPSC amplitude was 230±6pA before pairings and was increased by ~67% to 383±5pA one hour after pairings). Bottom, time course of Ri (baseline: 114±1MΩ and 50-60 min after pairings: 116±1MΩ; change of 1%). (**E**) Example of the lack of plasticity after 10 post-pre pairings (Δt_{STDP}=-12±0.2ms) with K252a (200nM) (the mean baseline EPSC amplitude was 147±5pA before pairings and a tLTD induction was observed one hour after 10 post-pre pairings: 106±3pA). Bottom, time course of Ri (baseline: 64±1 MΩ and 50-60 min after pairings: 59±1MΩ; change of 8%). **(F)** Example of the lack of plasticity after 10 post-pre pairings (Δt_{STDP}=-13±0.3ms) in presence of ANA12 (10μM) (the mean baseline EPSC amplitude was 198±4pA before pairings and was not significantly altered one hour after

pairings, 186±4pA). Bottom, time course of Ri (baseline: 74±0.2MΩ and 50-60 min after pairings: 68±0.2MΩ; change of 8%).

Insets correspond to the average EPSC amplitude during baseline (1, black trace) and the last 10 min of recording after STDP pairings (2, grey trace). Statistics (student t-test, first vs last 10 min of recording): ** $p<0.01$; *** $p<0.001$; ns, not significant.

Supplementary Figure 2: Calcium transients in dendritic spines remain unchanged upon ANA12 and DMSO applications (related the main Figure 4).

(**A**) ANA12 and ANA12 followed by DHF application did not change the time course of Ca2+ elevations triggered by somatic current injections eliciting two bAPs in dendritic spines and shafts. (**B**) Two consecutive applications of DMSO (DMSO1 and DMSO2, 0.04% final concentration)), to mimic successive applications of DHF and DHF+ANA12, did not change the time course of Ca2+ elevations in dendritic spines and shafts, triggered by two bAPs. (**C**) ANA12 and ANA12 followed by DHF application did not change the time course of Ca^{2+} elevations triggered by pre-post paired corticostriatal stimulations in dendritic spines and shafts. Error bars represent the SEM. ns, not significant.

Supplementary Figure 3: Long-duration bath-applied DHF did not promote tLTP for 25 post-pre pairings.

Averaged time-courses showing the absence of plasticity observed after 25 post-pre pairings with DHF bath-applied during the whole recording (2/5 cells showed tLTP). Error bars represent the SEM. Statistics (student t-test, first vs last 10 min of recording): ns, not significant.

Figure 1

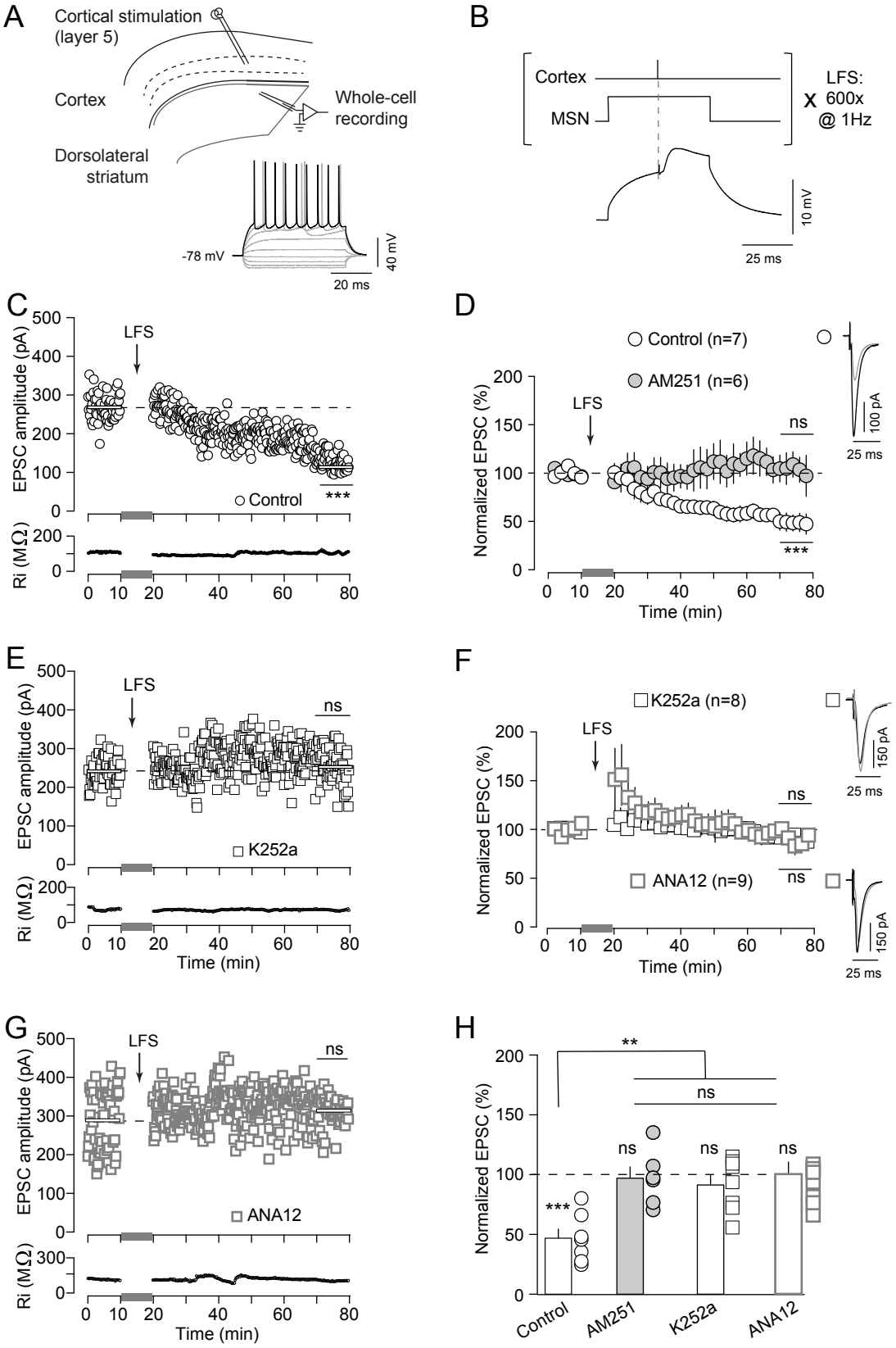
A
Cortical stimulation
(layer 5)
Cortex
Whole-cell
recording
Dorsolateral
striatum
-78 mV
40 mV
20 ms
B
Cortex
MSN
LFS:
x 600x
@ 1Hz
10 mV
25 ms
C
EPSC amplitude (pA)
LFS
Control
***
Ri (MΩ)
D
Control (n=7)
AM251 (n=6)
Normalized EPSC (%)
LFS
ns
***
100 pA
25 ms
Time (min)
E
EPSC amplitude (pA)
LFS
ns
K252a
Ri (MΩ)
Time (min)
F
K252a (n=8)
Normalized EPSC (%)
LFS
ns
ANA12 (n=9)
ns
150 pA
25 ms
Time (min)
G
EPSC amplitude (pA)
LFS
ns
ANA12
Ri (MΩ)
Time (min)
H
Normalized EPSC (%)
**
ns
***
ns
ns
ns
Control
AM251
K252a
ANA12

Figure 2

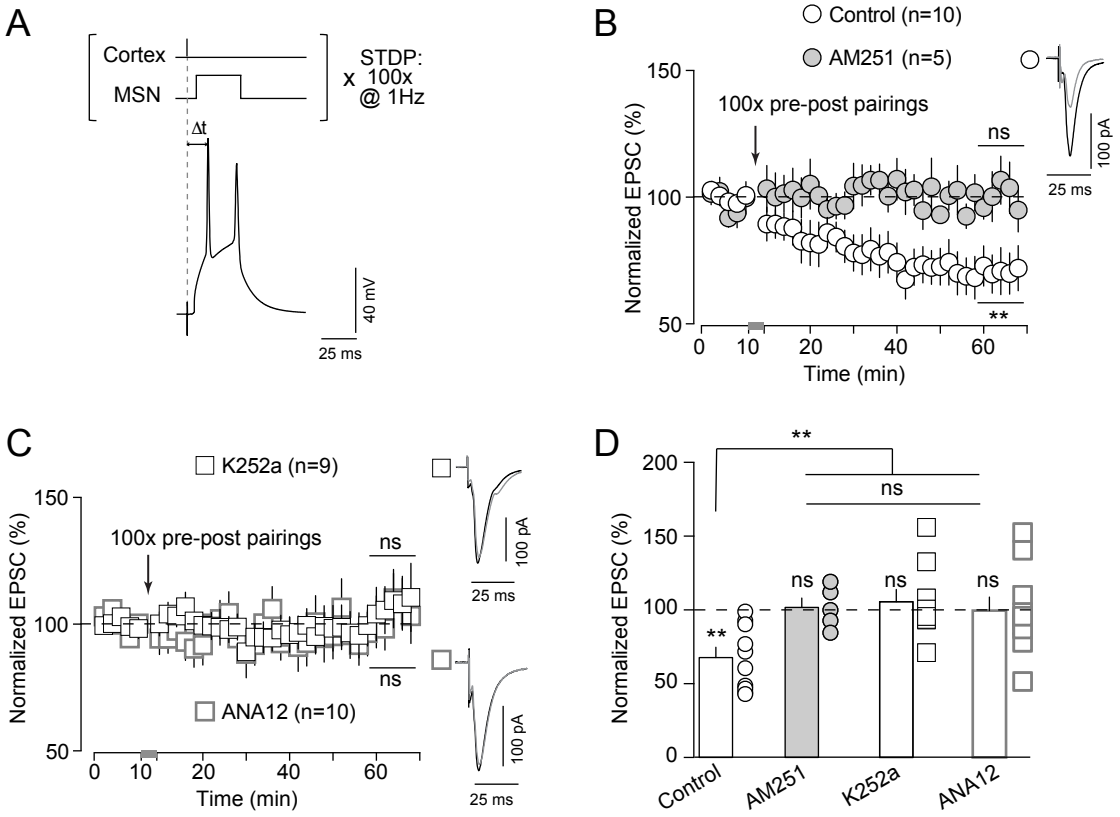
A
Cortex
MSN
STDP:
x 100x
@ 1Hz
Δt
40 mV
25 ms
B
Control (n=10)
AM251 (n=5)
100x pre-post pairings
ns
**
Normalized EPSC (%)
Time (min)
100 pA
25 ms
C
K252a (n=9)
ANA12 (n=10)
100x pre-post pairings
ns
Normalized EPSC (%)
Time (min)
100 pA
25 ms
D
**
ns
Normalized EPSC (%)
Control
AM251
K252a
ANA12

Figure 3

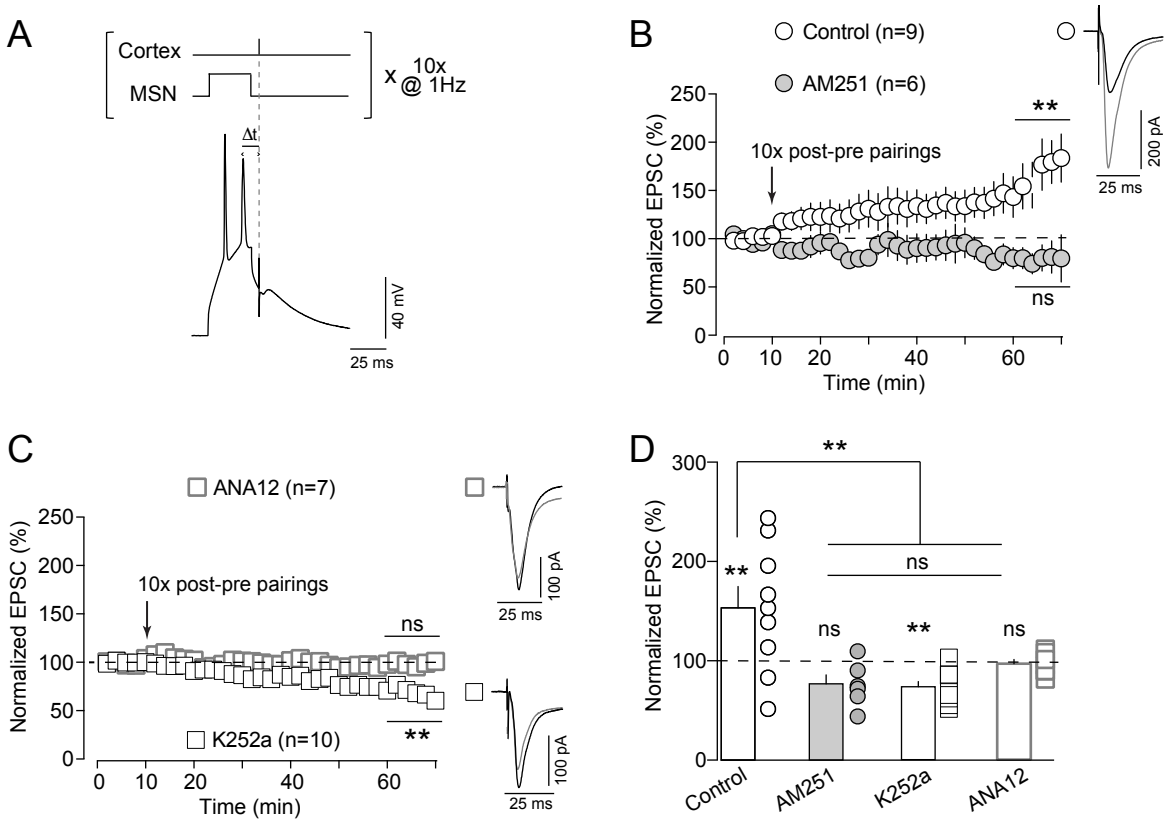
A
Cortex
MSN
x 10x @ 1Hz
Δt
40 mV
25 ms
B
Control (n=9)
AM251 (n=6)
10x post-pre pairings
Normalized EPSC (%)
Time (min)
**
ns
200 pA
25 ms
C
ANA12 (n=7)
K252a (n=10)
10x post-pre pairings
Normalized EPSC (%)
Time (min)
ns
**
100 pA
25 ms
D
Normalized EPSC (%)
Control
AM251
K252a
ANA12
**
ns

Figure 4

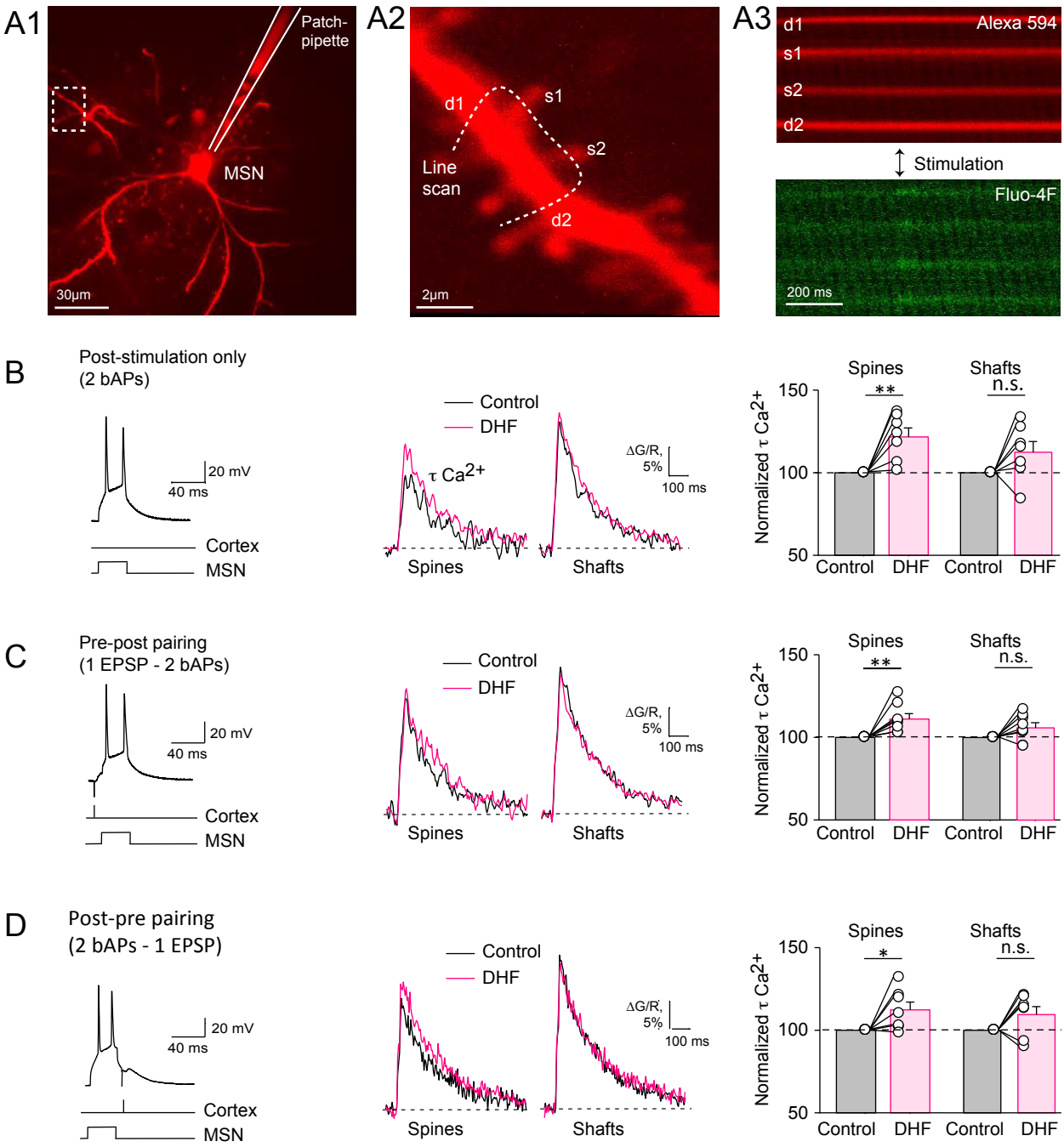
A1
Patch-pipette
MSN
30µm
A2
d1
s1
s2
d2
Line scan
2µm
A3
d1
s1
s2
d2
Alexa 594
Stimulation
Fluo-4F
200 ms
B
Post-stimulation only
(2 bAPs)
20 mV
40 ms
Cortex
MSN
Control
DHF
τ Ca2+
ΔG/R, 5%
100 ms
Spines
Shafts
Spines
Shafts
**
n.s.
Normalized τ Ca2+
150
100
50
Control
DHF
Control
DHF
C
Pre-post pairing
(1 EPSP - 2 bAPs)
20 mV
40 ms
Cortex
MSN
Control
DHF
ΔG/R, 5%
100 ms
Spines
Shafts
Spines
Shafts
**
n.s.
Normalized τ Ca2+
150
100
50
Control
DHF
Control
DHF
D
Post-pre pairing
(2 bAPs - 1 EPSP)
20 mV
40 ms
Cortex
MSN
Control
DHF
ΔG/R, 5%
100 ms
Spines
Shafts
Spines
Shafts
*
n.s.
Normalized τ Ca2+
150
100
50
Control
DHF
Control
DHF

Figure 5

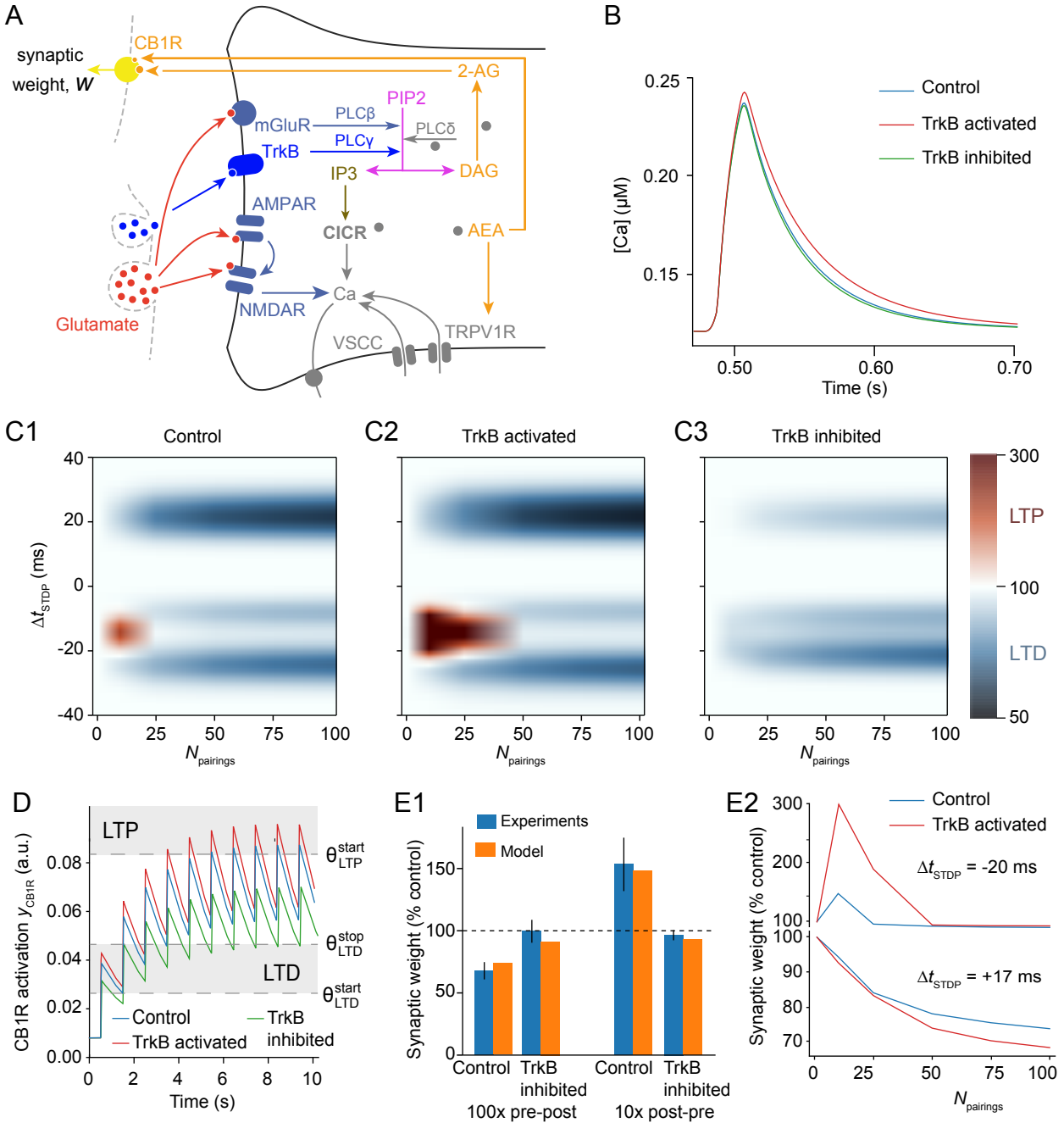
A
synaptic weight, W
CB1R
2-AG
PIP2
mGluR
PLCβ
PLCδ
TrkB
PLCγ
IP3
DAG
AMPAR
CICR
AEA
Ca
NMDAR
Glutamate
VSCC
TRPV1R
B
Control
TrkB activated
TrkB inhibited
[Ca] (μM)
Time (s)
C1
Control
C2
TrkB activated
C3
TrkB inhibited
Δt_STDP (ms)
N_pairings
LTP
LTD
D
LTP
LTD
CB1R activation y_CB1R (a.u.)
Time (s)
Control
TrkB activated
TrkB inhibited
E1
Experiments
Model
Synaptic weight (% control)
Control
TrkB inhibited
100x pre-post
10x post-pre
E2
Control
TrkB activated
Δt_STDP = -20 ms
Δt_STDP = +17 ms
Synaptic weight (% control)
N_pairings

Figure 6

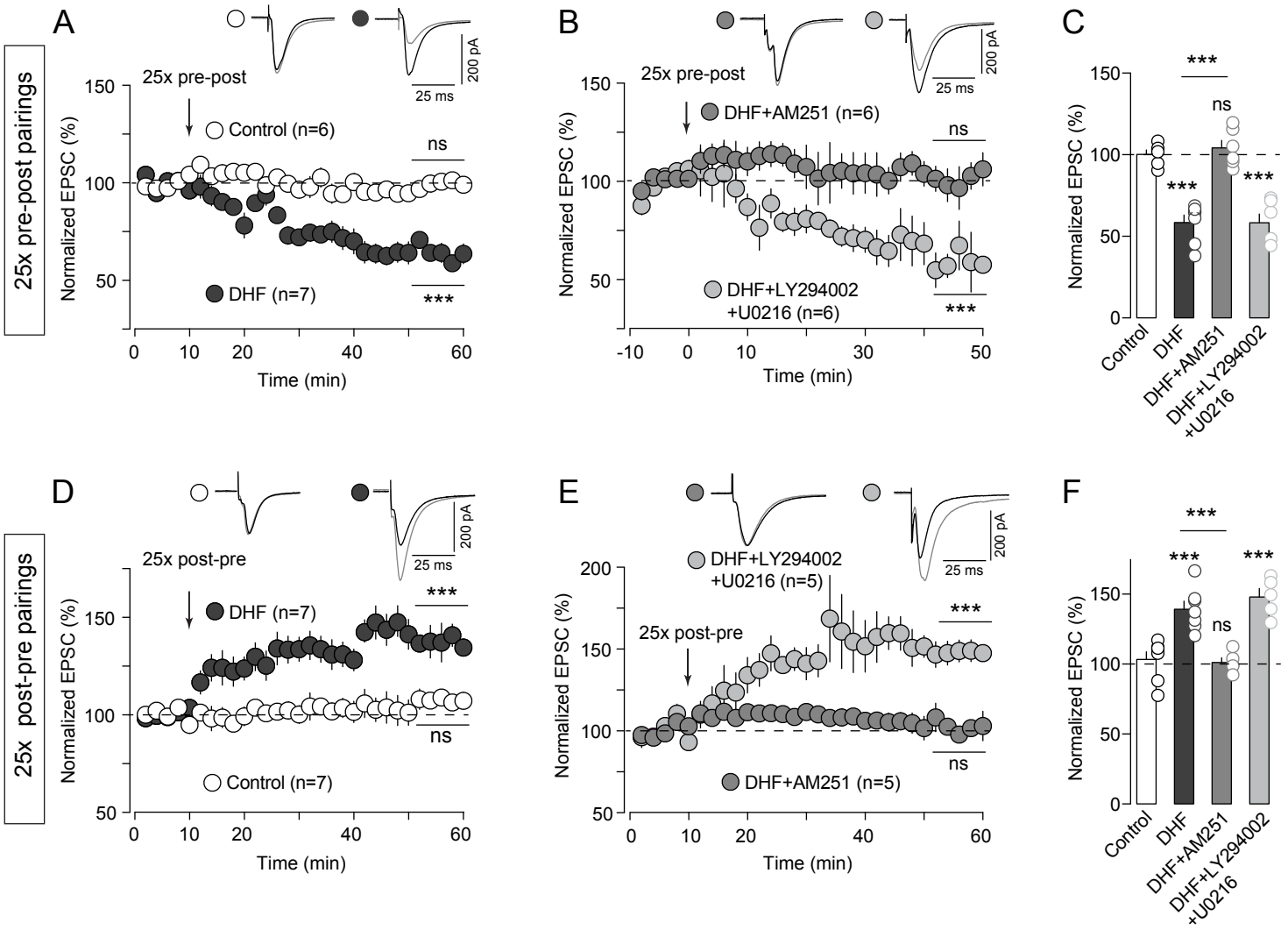
A
25x pre-post pairings
25x pre-post
Control (n=6)
DHF (n=7)
ns
***
Normalized EPSC (%)
Time (min)
200 pA
25 ms
B
25x pre-post
DHF+AM251 (n=6)
DHF+LY294002
+U0216 (n=6)
ns
***
C
Control
DHF
DHF+AM251
DHF+LY294002
+U0216
D
25x post-pre pairings
25x post-pre
DHF (n=7)
Control (n=7)
E
DHF+LY294002
+U0216 (n=5)
DHF+AM251 (n=5)
F